IDENTIFICATION OF A REGIONALLY COHERENT SUBSEASONAL SIGNAL OF STABLE ISOTOPES IN TROPICAL ANDEAN PRECIPITATION

A Thesis
by
HEATHER GUY

Submitted to the Graduate School
at Appalachian State University
in partial fulfillment of the requirements for the degree of
MASTER OF ARTS

August 2018
Department of Geography & Planning

IDENTIFICATION OF A REGIONALLY COHERENT SUBSEASONAL SIGNAL OF STABLE ISOTOPES IN TROPICAL ANDEAN PRECIPITATION

A Thesis
by
HEATHER GUY
August 2018

APPROVED BY:

L. Baker Perry, Ph.D.
Chairperson, Thesis Committee

Anton Seimon, Ph.D.
Member, Thesis Committee

Bronwen L. Konecky, Ph.D.
Member, Thesis Committee

Kathleen Schroeder, Ph.D.
Chairperson, Department of Geography & Planning

Max C. Poole, Ph.D.
Dean, Cratis D. Williams School of Graduate Studies

Abstract

IDENTIFICATION OF A REGIONALLY COHERENT SUBSEASONAL SIGNAL OF STABLE ISOTOPES IN TROPICAL ANDEAN PRECIPITATION

Heather Guy
MSci., Lancaster University
M.A., Appalachian State University

Chairperson: L. Baker Perry Ph.D.

Tropical Andean glaciers are rapidly retreating. Understanding how the climate has changed here in the past is key to understanding its future. Limited observations and the lack of comprehensive understanding of the controls on the isotopic (δD, $\delta^{18}O$) content of precipitation severely limit paleoclimate reconstructions in this region. This study examines four years of daily observations of δD and $\delta^{18}O$ in precipitation from ten sites in southern Peru and northern Bolivia and focuses on understanding the controls on the subseasonal spatiotemporal variability in $\delta^{18}O$ during the wet season. These data provide new insights into modern $\delta^{18}O$ variability at high spatial and temporal scales in light of recent developments in the field and in our understanding precipitation delivery in this region. We identify a robust, regionally coherent subseasonal signal of $\delta^{18}O$ in precipitation that occurs each year with a periodicity of ~15 days. This signal reflects variability in precipitation delivery driven by synoptic conditions, and closely relates to variations in the strength and direction of the South American

Low Level Jet and moisture availability directly to the east of the Altiplano. Annual layer snowpacks on high Andean glaciers retain this subseasonal signal, allowing the development of snow-pit age models based on precipitation $\delta^{18}O$ measurements and demonstrating that region-wide synoptic signals are recorded in the snow. This result has implications for improving paleoclimate reconstructions from tropical Andean ice cores and other paleoclimate records.

Acknowledgments

This work would not have been possible without the extensive team of people who have been a part of our fieldwork in South America. I would like to thank all participants in our field efforts 2009-17, all of our citizen scientist observers in Peru and Bolivia and our University partners at UNSAAC-Cusco and UMSA-La Paz. Thanks to Erik Pollock at the University of Arkansas Stable Isotope Lab for analyzing samples. This work is primarily funded by US National Science Foundation P2C2 Grant AGS 1566450. I have also received funding though the US National Science Foundation Grant AGS-1347179 (CAREER: Multiscale Investigations of Tropical Andean Precipitation) and from the Stephen Vacendak Graduate Fellowship in Geography, without which it would not have been possible for me to come to Appalachian State University (ASU). I would like to thank Bronwen Konecky for her guidance and for several interesting discussions. I would like to thank Anton Seimon, for his unfailing support and encouragement throughout my time at ASU, for his mentorship and for sharing his ideas that provided the inspiration for this thesis. Finally, I would like to thank Baker Perry, who made it possible for me to be here in the first place and continued to find a way for me to achieve everything that I wanted from my time at ASU. His guidance and support have been invaluable. Never have I come across an academic advisor more dedicated to the success of his students.

Table of Contents

Abstract iv

Acknowledgments vi

List of Tables viii

List of Figures ix

Foreword xiii

Introduction xiv

Article: *Identification of a Regionally Coherent Subseasonal Signal of Stable Isotopes in Tropical Andean Precipitation* 1

1. Introduction 3
2. Background and Literature Synthesis 5
3. Data and Methods 17
4. Results 19
5. Discussion 28
6. Conclusions 37
7. Appendix 38

References 38

List of tables 48

List of figures 53

Vita 71

List of Tables

Table 1. Characteristics of each of the stations and samples that were collected during the period used to analyze spatial variability (6 Dec 2016 to 30 Apr 2017). SD stands for standard deviation. Stations with asterisks are located in the Cordillera Real; all other stations are located in the Cordillera Vilcanota. There is no mean precipitation value for Chillca and Phinaya because these observers did not record non-measurable precipitation events and Chillca did not record most events < 5mm. 49

Table 2. Details of annual layer snowpits sampled in 2017 50

Table 3. Correlation matrix showing Pearson's product moment correlation coefficients between the 3-day precipitation weighted mean $\delta^{18}O$ at each station between 6 Dec 2016 and 30 Apr 2017. All correlations are significant at the 99% confidence interval 51

Table 4. Correlation matrix showing the Pearson's product moment correlation coefficients between the time series of 2017 $\delta^{18}O$ anomalies and variables from ERA-Interim reanalysis (15-day moving average minus the subseasonal signal). Variables: r = relative humidity, t = temperature, z = geopotential height, cc = cloud cover fraction, u = zonal wind. The numbers beside each variable refer to the level in the atmosphere (hPa). Correlations that are significant at the at the 99% confidence interval are highlighted with an asterisks. 52

List of Figures

Figure A1. Temporal progression of synoptic conditions associated with -1_2017 (26 Dec 2016 to 12 Jan 2017). Conditions averaged over the 6 days preceding (A-C), centered on (D-F) and after (G-I) the event. First column (A,D,G): 250 hPa geopotential heights (contoured) and winds. Second column (B,E,H): 850 hPa geopotential heights (contoured) and winds. Third column (C,F,I): 500 hPa relative humidity and winds. The black star shows the location of Quelccaya 55

Figure A2. The same as A1 but for -2_2017: 22 Feb 2017 to 7 Mar 2017 56

Figure A3. The same as A1 but for -3_2017: 19 Mar 2017 to 4 Apr 2017 57

Figure A4. The same as A1 but for +1_2017: 12 Dec 2016 to 22 Dec 58

Figure A5. The same as A1 but for +2_2017: 21 Jan 2017 to 14 Feb 59

Figure A6. The same as A1 but for +3_2017: 12 Apr 2017 to 24 Apr 2017.....................60

Figure 1. Study area. Left panel: the locations of the Cordilleras Vilcanota and Real, the four snowpit sampling locations (blue triangles) and the locations of the nearby cities of Cusco and La Paz (white stars). Right panel: key features of South American circulation discussed in this study. SACZ = South Atlantic Convergence Zone, SALLJ = South American Low Level Jet...61

Figure 2. Locations of precipitation collection sites. The table inset lists station names, elevations (msl) and the start date of each record...62

Figure 3. $\delta^{18}O$ and δD of each daily precipitation sample used in this study (2014-2017). Different shapes/ colors correspond to different stations (see legend inset). Samples with

a d-excess < 0 ‰ and precipitation amount < 25 mm are not included (see explanation in section 3). The global meteoric water line is plotted for comparison (black line) 63

Figure 4. Time series of $\delta^{18}O$ in all precipitation samples (2014-2017 = A-D respectively). Samples are plotted from August to August and each year is labeled after the year in which the wet season finishes. Although August does not necessarily reflect the transition between wet and dry seasons, it allows us to focus on the wet season and is sufficient for the purpose of this study. We use this naming convention in the rest of this paper. Samples from different stations are plotted in different colors (see legends inset). Solid lines join samples collected on consecutive days. The dashed blue line marks the average $\delta^{18}O$ each year (included in the legend) 64

Figure 5. A) $\delta^{18}O$ of all precipitation samples collected in 2017 (points, see legend inset), 3-day precipitation weighted mean of all samples (solid black line), 15-day moving average of the 30-day signal (dot-dash, green line, referred to as the subseasonal signal in this study) and the 90-day moving average of the 3-day signal (dashed, orange line, referred to as the seasonal cycle in this study). B) Subseasonal $\delta^{18}O$ anomalies during the 2017 wet season (subseasonal signal minus the seasonal cycle). Red shading highlights positive anomalies where the $\delta^{18}O$ anomaly is above the 75th percentile for at least 5 days and blue shading highlights negative anomalies where the $\delta^{18}O$ anomaly is below the 25th percentile for at least 5 days 65

Figure 6. Difference between positive and negative $\delta^{18}O$ anomalies in 2017. (A) and (B) show 250 hPa geopotential heights (contoured) and winds averaged over all of the postive anomalies and all of the negative anomalies respectively. (C) and (D) are difference plots, showing the average over all positive anomalies minus the average of all

negative anomalies for 500 hPa relative humidity and 500hPa cloud cover respectively. Black dots on the different plots show areas where the difference is significant at the 99% confidence interval. (E) and (F) show 850 hPa geopotential heights (contoured) and winds averaged over all of the positive anomalies and all of the negative anomalies respectively. The black star on each plot shows the location of Quelccaya in the Cordillera Vilcanota 66

Figure 7. 2017 time series of anomalies in (A) 500 hPa relative humidity, (B) 500 hPa cloud fraction and (C) 250 hPa zonal wind (solid blue line). Each anomaly series is calculated by subtracting the 90-day moving average (seasonal cycle) from the 15-day moving average of each field from ERA-Interim data averaged over the region 18.5˚ to 12˚ S and 74˚ to 65˚ W. The time series of $\delta^{18}O$ anomalies is overlaid on each plot for comparison (grey dashed line) 67

Figure 8. $\delta^{18}O$ anomaly plots for each wet season calculated in the same way as in Fig. 5b: (A) 2014, (D) 2015, (G) 2016. Adjacent to each anomaly plot are spatial plots of 500 hPa relative humidity and 850 hPa winds averaged over each negative anomaly (B,E,H) and each positive anomaly (C,F,I) for each respective year. The black star on each spatial plot shows the location of Quelccaya 68

Figure 9. Pearson's product-moment correlation coefficients between the time-series of $\delta^{18}O$ anomalies and time-series of 500hPa relative humidity anomalies at every grid-point for each year. Black dots highlight areas where the correlation is significant at the 99% confidence level. On each plot the black star shows the location of Quelccaya................69

Figure 10. $\delta^{18}O$ profiles of the annual layer snowpits on Quelccaya (A) and Huayna Potosí (B) sampled in July 2017. Overlain on each snowpit profile is the 15-day moving average $\delta^{18}O$ signal observed in region-wide precipitation, scaled to the liquid water equivalent depth in each snowpit from precipitation measurements from Quelccaya (A) and Chacaltaya (B), (red dashed line). Blue triangles are plotted every 5 days showing the snowpit age model. Vertical blue lines are plotted on the first day of each month. 70

Foreword

The main body of this thesis is formatted to the guidelines for manuscript submission to the *Journal of Hydrometeorology*, an official journal of the American Meteorological Society.

Introduction

Andean glaciers in Peru and Bolivia are rapidly retreating (Rabatel et al. 2013; Vuille et al. 2017) and unique information about the history of the climate in this region that has been preserved for centuries is in danger of being lost. Uncertainty still exists in the interpretation of climate signals from tropical Andean ice cores, in particular the interpretation of stable water isotopes (Vimeux et al. 2009). There is potential for new insights about historical climate change timing and mechanisms to be gained from these records, particularly with the introduction of new, ultra-high-resolution (μm) sampling technology that has the ability to examine chemical profiles on a sub-seasonal scale (Mayewski et al., 2014). To understand the climate signal recorded by sub-seasonal variations of $\delta^{18}O$ preserved in tropical ice cores it is necessary to understand the processes that control $\delta^{18}O$ in precipitation and how they are recorded in the snow. It is important to do this before any more information is lost as deglaciation and accelerating melt deplete the high Andean glacial archives.

The purpose of this study is to investigate how subseasonal variations of stable water isotopes in modern precipitation are controlled by meteorological processes and how these signals are preserved in high-altitude snowpacks. This study expands beyond previous work by providing additional observational data over a broad spatial and temporal scale. Four years of water isotope observations collected by citizen scientist observers on a daily basis at locations in the Cordillera Vilcanota, Peru, and the Cordillera Real, Bolivia are presented, allowing the assessment of spatiotemporal variability of water isotopes in precipitation at different scales. The role of local, regional and continental meteorological processes in controlling this variability is assessed using data from ERA-Interim: A global atmospheric reanalysis model with an 80 km spatial resolution.

Evidence of regionally coherent subseasonal oscillations in precipitation isotopes (δD, $\delta^{18}O$) demonstrates that they are recording a region-wide synoptic signal. Results from the analysis of ERA-Interim data show that periods where precipitation is more depleted in O^{18} relate to an increase in regional relative humidity and cloud cover associated with a strengthening of the South American Low Level Jet. Periods where precipitation is more enriched in O^{18} occur when the South American Low Level Jet is weakened or reversed or when there is limited moisture availability in the Amazon basin directly to the east of the study area. The cycle between these two states has a periodicity of ~15 days and is associated with continental scale precipitation variability related to the movement of the South Atlantic Convergence Zone. This signal is clearly retained in isotopic profiles from annual layer snowpits in both Cordilleras. This result suggests that subseasonal variations in isotopes preserved in tropical Andean ice reflect regional circulation anomalies and that ice cores extracted from both of these Cordilleras are recording equivalent signals. This has important implications for improving the interpretation of isotopic signals in tropical Andean ice cores and is a first step towards being able to make subseasonal paleoclimate reconstructions. Future work will focus on investigating if this signal is also recorded in insoluble chemicals deposited in the snow that can be sampled at an ultra-high resolution in ice cores going back millennia.

This research project was a team effort and could not have been completed without our collaborators, observers and field assistants in Peru and Bolivia and everyone who has participated in data collection over the last four years. On the authorship list,

Heather Guy took a lead role in designing this study, assisted with the collection of samples in the field in July 2017, and completed all of the data analysis, figure generation, writing, and formatting of this manuscript. Anton Seimon provided invaluable guidance and expertise, played a major role in all data collection and contributed several of the ideas discussed in this study. Baker Perry enabled the completion of this work by facilitating and organizing fieldwork campaigns, providing financial and emotional support, playing a major role in all data collection and contributing some of the ideas discussed in this study. Bronwen Konecky took part in several fruitful discussions and provided a different perspective on isotope science that helped to form some of the ideas discussed in this study. Maxwell Rado coordinated our citizen scientist observers in Peru and Marcos Andrade coordinated our citizen scientist observers in Bolivia.

Identification of a Regionally Coherent Subseasonal Signal of Stable Isotopes in Tropical Andean Precipitation.

Heather Guy*, Anton Seimon and L. Baker Perry

Appalachian State University, Boone, North Carolina

Bronwen L. Konecky

Washington University in St. Louis, St. Louis, Missouri

Maxwell Rado

Universidad Nacional de San Antonio Abad del Cusco, Cusco, Peru

Marcos Andrade

Universidad Mayor de San Andrés, La Paz, Bolivia

**Corresponding author address:* Heather Guy, Department of Geography and Planning, P.O. Box 32066, Appalachian State University, Boone, North Carolina 28608

E-mail: guyh@appstate.edu

ABSTRACT

Tropical Andean glaciers are rapidly retreating. Understanding how the climate has changed here in the past is key to understanding how it will change in the future. Limited observations and the lack of comprehensive understanding of the controls on the isotopic (δD, δ^{18}O) content of precipitation severely limit paleoclimate reconstructions in this region. This study examines four years of daily observations of δD and δ^{18}O in precipitation from ten sites in southern Peru and northern Bolivia and focuses on understanding the controls on the subseasonal spatiotemporal variability in δ^{18}O during the wet season. These data provide new insights into modern δ^{18}O variability at high spatial and temporal scales in light of recent developments in the field and in our understanding precipitation delivery in this region. We identify a robust, regionally coherent subseasonal signal of δ^{18}O in precipitation that occurs each year with a periodicity of $\sim$15 days. This signal reflects variability in precipitation delivery driven by synoptic conditions, and closely relates to variations in the strength and direction of the South American Low Level Jet and moisture availability directly to the east of the Altiplano. Annual layer snowpacks on high Andean glaciers retain this subseasonal signal, allowing the development of snow-pit age models based on precipitation δ^{18}O measurements and demonstrating that region-wide synoptic signals are recorded in the snow. This result has implications for improving paleoclimate reconstructions from tropical Andean ice cores and other paleoclimate records.

1. Introduction

With an average elevation of nearly 4000 m, the Andes form a significant barrier to atmospheric flow and play a large role in modulating the weather and climate of western South America. In southern Peru and northern Bolivia (12° S to 16° S; Fig.1) the Andes reach their widest point, the Altiplano: a high plateau with a north-west to south-east orientation, bordered by cordilleras on the eastern and western flanks. This region of the Andes is very sensitive to climate change, and as rapid glacial loss threatens water resources (Rabatel et al. 2013; Vuille et al. 2017), it is increasingly important to understand how the climate in the outer tropical Andes has changed in the past in order to prepare for the future. The disappearing glaciers also mean that the time available to study glacial processes and to extract paleoclimate records is limited (Thompson et al. 2017).

This study focuses on the Cordillera Vilcanota and the Cordillera Real on the north-eastern edge of the Altiplano (Fig.1). The Cordillera Vilcanota is home to the Quelccaya Ice Cap, the world's largest tropical glacier and the site of one of the most important ice core records in the tropical Andes. The ice core extracted from Quelccaya in 2003 is annually resolvable for the last 1,800 years and has been used to reconstruct past changes in Pacific sea surface temperatures, migration of the Intertropical Convergence Zone and conditions during the Little Ice Age (Thompson et al. 2013). In the Cordillera Real, an ice core extracted from Nevado Illimani in 1999 dates back 18,000 years and contains information about tropical Andean climate changes that occurred during the transition from the Last Glacial Stage to the Holocene (Ramirez et al. 2003). There are ongoing projects to extract new cores from both the Cordillera Real and the Cordillera Vilcanota, and recent advances in ice core laser sampling technology will enable researchers to sample new cores at an unprecedented (μm) resolution with thousands of sample points per annual layer (Mayewski et al. 2014).

Commonly measured in ice cores are the relative concentrations of the rare stable isotopes ^{18}O and ^{2}H relative to the concentrations of ^{16}O and ^{1}H (hereafter referred to as water isotopes), which are closely related to the isotopic composition of precipitation at the time of accumulation. Meteorological and climatological conditions control water isotopes in precipitation, so identifying these controls is essential to understanding the climate signal preserved in ice cores and other paleoclimate records. In polar regions, a robust relationship between surface temperature and concentrations of ^{18}O isotopes allows for reconstructions of historical temperature. Thompson (2000) suggested that a similar relationship might be used to make temperature reconstructions from tropical ice cores, however, different meteorological regimes and moisture transport processes complicate this relationship in tropical regions (Dansgaard 1964) and uncertainty still exists in the interpretation of water isotopes recorded in tropical Andean ice cores (Vimeux et al. 2009). To understand the climate signal preserved by isotopic tracers in ice cores we need to understand the modern day controls on the isotopic content of precipitation and how this signal is retained in the snow and ice.

Most studies in the tropical Andes to date have focused on understanding the controls on the monthly or interannual variations of water isotopes in precipitation (e.g., Gonfiantini et al. 2001; Vimeux et al. 2005; Vuille and Werner 2005; Insel et al. 2013; Fiorella et al. 2015). In this study, we focus on understanding the meteorological controls on the sub-monthly spatiotemporal variability. Understanding the controls on variability at subseasonal timescales has the potential to not only improve our understanding of the processes driving isotope variability in precipitation but is a first step towards making subseasonal reconstructions from ice cores and other paleoclimate records with annually resolvable strata. This work will be particularly applicable in the interpretation of isotopic signals from new ice cores in this region.

This study presents four years of daily measurements of water isotopes in precipitation from ten observation sites in the Cordillera Vilcanota and the Cordillera Real. The goal of this study is to improve our understanding of the dominant meteorological controls on the subseasonal variations of water isotopes in precipitation and how this signal is retained in the annual layer snowpack. A better understanding of these controls may be used to improve regional paleoclimate reconstructions, and by extension, our understanding of how the climate in the central Andes will change in the future.

2. Background and Literature Synthesis

a. What controls water isotopes in tropical precipitation?

The two most common naturally occurring stable water isotopologues $H_2^{18}O$ and ^2H_2O have a lower volatility than the lighter and more common $^1H_2^{16}O$, resulting in isotopic fractionation during all evaporation and condensation processes. For this reason, the isotopic composition of precipitation is an important hydrological tracer that encodes information about the source of the precipitation and its evaporation and condensation history. Water isotope composition is generally stated in parts per mille (‰) as relative deviations with respect to the VSMOW (Vienna Standard Mean Ocean Water), shown by equation (1) (Gonfiantini 1978).

$$\delta = \frac{R_x}{R_{VSMOW}} - 1 \tag{1}$$

R_x is the abundance ratio of species x and R_{VSMOW} is the standard abundance ratio of that species. Hereafter, I refer to the relative deviation of ^{18}O in water as δ^{18}O and the relative deviation of ^{2}H as δD.

The isotope-temperature relationship observed in polar regions does not hold in the tropics because the fundamental assumptions that explain this relationship no longer apply. In particular, complex precipitation delivery mechanisms in the tropics consisting of a mixture of isolated convective storms and mesoscale convective systems (MCSs) with complex structures mean that the kinetic effects that control the amount of isotopic fractionation are not uniform.

In convective storms, strong updrafts and downdrafts result in within-cloud re-evaporation and mixing of atmospheric layers with different isotopic compositions (Risi et al. 2008). Individual droplets grow in updrafts and will interact with all of these different layers as they fall back down through the cloud and coalesce with smaller water droplets that are still suspended. Below the cloud, a raindrop will undergo either total or partial re-evaporation and will be subject to equilibration with the surrounding vapor via molecular diffusion, altering the isotopic composition of the rain droplet itself and the surrounding vapor (Friedman et al. 1962; Dansgaard 1964; Stewart 1975; Field et al. 2010). Partial re-evaporation tends to enrich precipitation in heavy isotopes relative to its initial composition (Dansgaard 1954; Gat 2000; Risi et al. 2008). The effect of re-equilibration on the isotopic composition of precipitation depends on the isotopic composition of the below cloud vapor (Friedman et al. 1962). In the same way, precipitation falling through saturated layers or lower level clouds will have a modified isotopic composition (Liotta et al. 2006). This effect is common in mountainous regions where orographic enhancement of rainfall occurs via the seeder-feeder mechanism; where rain droplets from a higher level cloud fall through an orographically produced cap cloud, enhancing precipitation by coalescence (Houze 1993). In this case, modification of the isotopic composition of the initial precipitation can result in very different isotopic values from the isotopic composition of precipitation in surrounding areas (Liotta et al. 2006; Coplen et al. 2008).

Precipitation phase can also influence isotopic composition. The formation of ice crystals by vapor deposition usually occurs under super-saturated conditions leading to relatively more depleted precipitation (Jouzel and Merlivat 1984). Additionally, below cloud processes do not alter the isotopic composition of frozen precipitation on the timescales it takes for the precipitation to reach the ground resulting in relatively lower δ^{18}O when the melting layer is near the surface (Friedman et al. 1962; Gonfiantini et al. 2001).

Another important process is the re-evaporation of soil moisture from previous precipitation events that alters the isotopic composition of the boundary layer moisture. Because boundary layer moisture feeds convective updrafts, the initial isotopic composition of the water vapor is influenced by the amount of re-evaporation and moisture recycling in the time leading up to each precipitation event (Risi et al. 2008). In this way, successive storms in tropical regions might develop a memory effect were the initial isotopic composition of the vapor depends on the isotopic composition of precipitation in the previous storm (Field et al. 2010).

The relative importance of each of these effects depends on the depth of convection, cloud microphysical processes, storm duration, rain rate, droplet size and relative humidity. Despite these complications, δ^{18}O in tropical regions is widely observed to correlate with changes in precipitation amount on interannual (e.g., Hardy et al. 2003; Vuille et al. 2003; Insel et al. 2013) and seasonal (e.g., Dansgaard 1964; Rozanski et al. 1993; Vimeux et al. 2005; Fiorella et al. 2015) time scales. One way to interpret this effect relates to the feedback process described above, where the frequency and duration of storms alter the isotopic composition of low level moisture that feeds subsequent storms. More frequent and more intense convective events will cause the low-level moisture to become progressively more depleted as a result of the 'amount effect' (Risi et al. 2008; Vimeux et al. 2011).

Aside from these local processes, the initial isotopic composition of water vapor determines the baseline for the isotopic composition of precipitation and can vary considerably depending on conditions during evaporation at the original moisture source and any processes that occur during moisture transport. For this reason, changes in the isotopic composition of precipitation have been related to changes in moisture inflow trajectories (Aggarwal et al. 2004) and changes in rainout and moisture recycling upstream (e.g., Villacís et al. 2008). These processes are site specific; moisture transport pathways to the central Andes are discussed in Section 2b.

Aggarwal et al. (2012) proposed 'atmospheric moisture residence time', the ratio of total precipitable water to precipitation rate, as a parameter that can describe global interannual water isotope variations by incorporating the effects of changing temperature, moisture source and strength of the hydrologic cycle. However this study only included data from two relatively low-elevation tropical locations in Africa that are unlikely to be representative of conditions in the tropical Andes. On shorter timescales, several studies have found evidence of a relationship between δ^{18}O in tropical precipitation and the degree of organization of the precipitating system (Lawrence et al. 2004; Kurita et al. 2011; Kurita 2013; Aggarwal et al. 2016). Specifically, isolated convective storms are associated with relatively enriched precipitation compared to MCSs with extensive stratiform regions that are associated with more depleted precipitation. Aggarwal et al. (2016)

find a significant negative correlation between δ^{18}O in precipitation and stratiform fraction and attribute this to the different dynamical and microphysical processes involved with rainfall formation in different cloud types.

The controls on water isotopes in tropical precipitation are clearly complex with many possible mechanisms that might lead to an equivalent isotopic composition. A parameter that can help to delineate these mechanisms is the deuterium excess parameter (henceforth d-excess). δD is less sensitive to kinetic effects than δ^{18}O, it is therefore possible to detect, and to some extent diagnose, non-equilibrium processes by considering the relationship between δD and δ^{18}O (Dansgaard 1964). The Global Meteoric Water Line (GMWL), defined as $\delta D = 8\ \delta^{18}O + 10$ ‰, describes this relationship under equilibrium conditions. Variations from the GMWL occur due to kinetic processes and the d-excess parameter describes these variations, where d-excess = $\delta D - 8\delta^{18}O$. Small or negative d-excess can result from enrichment due to below cloud evaporation. Higher d-excess values can result from non-equilibrium condensation during the growth of ice crystals (Jouzel and Merlivat 1984) or continental moisture recycling (Gat and Matsui 1991). Deviations from the GMWL can also result from changes in moisture source region or changes in evaporation conditions at the moisture source region (Pfahl and Sodemann 2014).

b. The meteorological regime of the Altiplano

In order to understand how these processes work together to control the isotopic content of precipitation in the Cordillera Real and the Cordillera Vilcanota, it is important to understand the local and regional meteorology. In the Andes, in situ meteorological observations are relatively sparse and the complex topography causes large uncertainties in remotely sensed data (Dinku et al.

2008; Scheel et al. 2011). Despite this, understanding of the meteorology and climatology in the central Andes has improved signicantly over the last 20 years with the recognition of the sensitivity of mountain ecosystems to changes in precipitation, and with the need to understand precipitation variability in order to interpret paleoclimate records from tropical ice cores (Vimeux et al. 2009).

Key features of the climate of the tropical Andes are the distinct wet and dry seasons. In the northeastern Altiplano the wet season typically runs from November until March. The winter months (April to October) are extremely arid, and during this time glacial melt-water provides an essential buffer to water resources (Vergara et al. 2007). Due to the high elevation, the air above the Altiplano itself is very dry. Upslope flow along valleys connected to the Amazon basin driven by the heating of sloping terrain generates a large scale zonal circulation that transports moisture to the Altiplano from lower levels (Egger et al. 2005). The high solar irradiance results in the development of a conditionally unstable boundary layer over the Altiplano throughout the year; suggesting that moisture availability controlled by changes in moisture influx from the Amazon basin is the limiting factor to precipitation in this region (Garreaud 1999; Garreaud et al. 2003). Changes in upper level zonal flow modulate the strength and duration of this moisture transport. In Austral winter, the subtropical Westerly jet reaches its most northerly position in response to the temperature contrast between the tropics and the mid-latitudes, resulting in a mean westerly upper level flow over the Altiplano, inhibiting moisture transport (Garreaud et al. 2003). Precipitation events that occur during this time appear to relate to midlatitude disturbances tracking abnormally far north (Vuille and Ammann 1997).

In austral summer, the zone of peak insolation shifts southward resulting in a weakening and southward shift of the subtropical westerly jet, a southward expansion of the equatorial easterly trade winds and enhanced convection over the Amazon Basin. The mean upper level flow over the Altiplano switches to an easterly direction, enhancing moisture transport onto the Altiplano from the Amazon basin and resulting in precipitation (Garreaud et al. 2003). In response to the low pressure that forms over the Amazon as a result of enhanced convection, the Bolivian High, an upper tropospheric anticylonic circulation centered at approximately 15°S, 65°W, is established (Lenters and Cook 1999).

Several studies have linked the strength and position of the Bolivian High to intraseasonal variability of precipitation over the Altiplano (Aceituno and Montecinos 1993; Lenters and Cook 1999; Vuille 1999). When the Bolivian high strengthens and expands poleward, the upper level easterly flow over the Altiplano strengthens coinciding with enhanced precipitation. When the Bolivian High weakens and migrates northward, the upper level easterly flow over the Altiplano weakens coinciding with reduced precipitation. However, it is difficult to disentangle whether it is the latent heating due to enhanced precipitation that is causing the Bolivian high to strengthen, whether the strengthening of the Bolivian high causes the enhanced precipitation or whether both of these processes are true and a positive feedback system develops (Lenters and Cook 1999). In any case, wet season precipitation over the Altiplano is inherently episodic. Wet periods, typically 5-20 days long, alternate with dry periods of a similar duration (Lenters and Cook 1997; Garreaud 1999, 2000). Despite the complex terrain, these wet and dry periods are typically regionally coherent (Garreaud 2000; Perry et al. 2014; Hurley et al. 2015).

The majority of moisture reaching the Altiplano ultimately originates from the western Atlantic Ocean and undergoes considerable recycling due to convective precipitation and evapotranspiration over the Amazon before its arrival (Grootes et al. 1989). Low-level easterly trade winds are deflected southwards where they meet the Andean mountain barrier, accelerating to form the South American Low Level Jet (SALLJ), which reaches maximum velocity close to the 850 hPa level as it runs north-westerly to the east of the Altiplano in Bolivia (Vera et al. 2006). Studies investigating the moisture inflow trajectories to the northeastern Altiplano and the eastern Cordilleras have demonstrated that the majority of precipitation events arrive under weak flow along north-westerly trajectories that originated in the north Atlantic (Vimeux et al. 2005; Insel et al. 2013; Perry et al. 2014). However recent studies have also identified that some moisture arrives at the central Andes along southeastern trajectories that ultimately originate over the southern Pacific Ocean (Insel et al. 2013; Perry et al. 2014).

The subseasonal wet and dry periods on the Altiplano appear to relate to a number of different forcing mechanisms. One mechanism resulting in wet periods on the Altiplano occurs in association with the presence of an area of low pressure to the southeast of the Altiplano related to a propagating extratropical cyclone further south. This low pressure system is associated with a strengthening of the SALLJ that advects warm moist tropical air along the eastern edge of the Altiplano resulting in enhanced precipitation (Lenters and Cook 1999; Junquas et al. 2017). A second mechanism relates to a westerly shift of the South Atlantic Convergence zone (SACZ: a north-west to south-east oriented band of convection originating in the Amazon basin and associated with the South American Summer Monsoon) and an anomalous region of high pressure over the south central Amazon basin (Lenters and Cook 1999). This warm anomaly causes the Bolivian high to strengthen and shift southward and enhances the advection of warm moist air over the eastern slopes of the Altiplano. The variability in the SACZ has been linked with the Madden Julian Oscillation (MJO: Paegle et al. 2000; Alvarez et al. 2016). A different mechanism resulting in enhanced precipitation over the Altiplano relates to cold air incursions. In contrast to propagating waves of low pressure to the south east of the Altiplano associated with extratropical cyclones, cold air incursions are narrow bands of low pressure that extend as far north as Santa Cruz (Garreaud 1999). In the wet season, low level convergence ahead of the northwards propagating cold front of the cold air incursion strengthens the SALLJ and forms a band of organized convection (Garreaud 1999). The enhanced SALLJ and convection to the east of the Altiplano increases moisture transport and results in positive precipitation anomalies. Behind the cold front, there is a reversal of the SALLJ and cooler air originating from the extra tropics limits moisture availability resulting in periods of suppressed precipitation.

On the eastern cordilleras of the Altiplano, the daily cycle of precipitation during rainy periods in the wet season is typically bimodal, featuring a nighttime precipitation event that peaks around local midnight, and an afternoon precipitation event that peaks around 16:00 LST (Perry et al. 2014, 2017; Chavez and Takahashi 2017; Junquas et al. 2017). The late afternoon events are convective in nature and result from instability due to day-time heating of the lower atmosphere. The meteorological forcing associated with the night-time precipitation is an area of current research. Observations indicate that the nighttime precipitation events are regionally coherent and stratiform in structure (Perry et al. 2017). One proposed mechanism is that in the absence of thermal heating in the evening, winds flow down the eastern slope of the Andes leading to enhanced convection in the Andes-Amazon transition region. This convection eventually organizes into MCSs featuring extensive stratiform regions that spread both upslope and downslope (Chavez and Takahashi 2017) potentially resulting in the widespread nighttime precipitation observed on the Altiplano. Another study has demonstrated that the strength of the SALLJ modulates the moisture flux into the eastern Cordilleras of the Peruvian Altiplano by channeling moisture up northwest orientated valleys (Junquas et al. 2017). The SALLJ is strongest overnight (Garreaud and Wallace 1997; Marengo et al. 2004; Junquas et al. 2017) and Junquas et al. (2017) present evidence that the upslope flow forced by the SALLJ persists overnight. This moisture transport combined with the stable nighttime atmosphere may mechanically produce precipitation that is more stratiform in structure.

c. Variability of water isotopes in tropical Andean precipitation.

With the development of paleoclimate reconstructions based on δ^{18}O variability in tropical Andean ice cores (Thompson 2000), interest in the modern controls on water isotopes in central Andean precipitation has grown, and a number of observational studies have attempted to delineate the dominant controls on δ^{18}O in precipitation, snow and ice at different time scales. On interannual scales several studies have found that δ^{18}O is strongly correlated with precipitation amount (e.g., Vuille et al. 2003; Hardy et al. 2003; Hoffmann et al. 2003). However, this does not appear to be a straightforward relationship as local precipitation amount does not consistently explain δ^{18}O variations (Vuille and Werner 2005; Vimeux et al. 2005; Insel et al. 2013). In some locations low δ^{18}O occurs alongside negative local precipitation anomalies but enhanced upstream precipitation, implying an important role for moisture transport and upstream rainout processes (e.g., Vuille and Werner 2005). Interannual variations in precipitation amount relate to changes in Pacific sea surface temperatures and the phase of the El Niño Southern Oscillation (ENSO). This has led several studies to claim that δ^{18}O variations in ice cores record ENSO variability (e.g., Vuille et al. 2003; Hoffmann et al. 2003; Bradley et al. 2003; Hardy et al. 2003); however, the effect of ENSO phase on precipitation variability over the Cordillera Vilcanota and Cordillera Real remains unclear (Perry et al. 2014, 2017). Vuille and Werner (2005) demonstrated a negative correlation between δ^{18}O on the Altiplano and intensity of the South American Summer Monsoon (SASM), but because ENSO impacts the strength of the SASM (Zhou and Lau 2001) it is possible that ENSO dominates this signal. Insel et al. (2013) related interannual δ^{18}O variability in the north central Andes to changes in precipitation driven by large scale atmospheric circulation features. In particular they found a strong negative correlation between monthly δ^{18}O and regional precipitation amount related to the strength of the SALLJ. They also found a correlation between δ^{18}O and the number of days with trajectories from the north-west. A larger number of days with north-westerly trajectories are associated with a more southerly Bolivian high, and a higher number of trajectories from the south-east occur when the Bolivian high is in a more northerly position and are associated with more enriched precipitation (Insel et al. 2013).

Fiorella et al. (2015) do not find any correlation between the position of the Bolivian High and either δ^{18}O or precipitation amount on the Altiplano, despite a relationship between the Bolivian High and moisture source. Instead, they conclude that upstream precipitation anomalies are a more important factor contributing to δ^{18}O variability. Vimeux et al. (2005) came to a similar conclusion, showing δ^{18}O does not relate to local temperature or precipitation, but that rainout along upstream trajectories and convective activity over the Amazon basin are important. Both of these studies used monthly precipitation samples that are insufficient to capture the controls on the dominant mode of subseasonal precipitation variability over the Altiplano that occurs over a period of 10-40 days. Vimeux et al. (2011) use one year of event-based precipitation samples in the Zongo valley in Bolivia to demonstrate that intra-monthly variability in δ^{18}O exists and is consistent between stations despite large differences in elevation and local precipitation amounts. Vimeux et al. (2011) identify intraseasonal oscillations in δ^{18}O with a periods of 41, 18, 11 and 6 days that appear to be associated with variations in the position of the SACZ. An earlier modeling study also found evidence for this relationship (Sturm et al. 2007). However, as all of the sites that Vimeux et al. (2011) used are located in the same valley, this result does not indicate whether this a region wide signal or the result of precipitation at all stations originating from a single air mass.

Another important control on precipitation δ^{18}O in the Andes is the ‘altitude effect’. Under equilibrium conditions, continuous cooling and condensation as an air mass rises adiabatically over topography result in the preferential rainout of heavy water isotopes and more depleted precipitation at higher altitudes (Dansgaard 1964). Several studies have observed this effect over the Andes, particularly over the Andes-Amazon transition (e.g., Gonfiantini et al. 2001; Fiorella et al. 2015), leading to the suggestion that altitude might be the dominant driver of spatial δ^{18}O variability in the Andes (Fiorella et al. 2015). However, on the Altiplano itself the relationship between δ^{18}O and altitude is much weaker (Fiorella et al. 2015). In this study, we use samples collected between 3,300 m and 5,050 m and we observe little if any evidence of an altitude effect.

Finally a recent study focusing on δ^{18}O variability in snow and ice on Quelccaya presented evidence that subseasonal precipitation variability and δ^{18}O is associated with cold air incursions (Hurley et al. 2015). Positive precipitation anomalies and low δ^{18}O relate to MCSs that form along the equatorward edge of the cold air incursion. Cold dry air behind this front results in negative precipitation anomalies and higher δ^{18}O.

A lack of observations still limits our understanding of water isotope variability over the Altiplano and the eastern Codilleras. In particular there is a lack of daily measurements of isotopes in precipitation, and those that do exist have small spatial and temporal resolutions. Recent developments in our understanding of precipitation delivery mechanisms over the Altiplano, and in our understanding of the controls on tropical isotopic variability in general, suggest that a re-evaluation of the controls on subseasonal δ^{18}O variability over the Altiplano is necessary. With the extraction of new ice cores from this region and developments in high resolution ice core sampling technology, improving our understanding of the subseasonal controls on isotopes in precipitation could offer the potential to significantly improve regional paleoclimate reconstructions.

3. Data and Methods

This study presents daily measurements of water isotopes in precipitation from ten collection sites on the north-eastern edge of the Altiplano, seven in the Cordillera Vilcanota region and three in the Cordillera Real (Fig. 2). Trained observers take liquid equivalent precipitation measurements each morning at 0700 LST (1200 UTC in the Cordillera Vilcanota and 1100 UTC in the Cordillera Real) using established protocols (Doesken and Judson 1997; Cifelli et al. 2005). On days where there is sufficient precipitation (>0.5 mm), observers collect a sample from the gauge and seal it in a glass vial. The University of Arkansas Stable Isotope Laboratory analyzed these samples for their isotopic composition (δD, δ^{18}O), the approximate uncertainty is $\pm$1 ‰ for the δD samples and $\pm$0.5 ‰ for the δ^{18}O samples. Observers at Murmurani and Pucarumi began collecting samples in 2013, the remaining sites began taking measurements in 2016 or early 2017.

A limitation of this sampling protocol is the possibility that morning or afternoon precipitation events might be subject to evaporation in the rain gauge (and therefore isotopic enrichment) prior to collection the following morning. Field tests in the Cordillera Vilcanota in July 2017 showed that a 2 to 7 ‰ increase in δ^{18}O occurred in small precipitation samples (approximately 4 mm) that were left out in gauges between 1400 LST and 0700 LST, but no significant enrichment occurred in larger samples (approximately 25 mm) or samples that were only left out overnight. The samples that underwent evaporative enrichment were clearly identifiable by low d-excess values (d-excess < 0 ‰). To account for this bias, we removed all samples with precipitation less than 25 mm and d-excess values of less than 0 ‰ prior to analysis.

Section 3a and 3b give an overview of the data. Section 3c assesses the spatial variability of δ^{18}O in the study area by comparing all samples collected between 6 December 2016 and 30 April 2017. This covers the majority of the 2017 wet season, during which there are daily samples from seven sites, including two sites in the Cordillera Real (Table 1). Cota Cota and Sallayoc are not included in this analysis because the observers did not start collecting samples until late January 2017. A correlation matrix was built using 3-day precipitation weighted means of δ^{18}O for each site. Linear interpolation was used to estimate δ^{18}O values on days were no precipitation occurred. The weight assigned to each day was the precipitation amount recorded on that day. Using a 3-day running mean smooths out the highest frequency of variability and fills the gaps in the data.

Data from ERA-Interim reanalysis, a global atmospheric reanalysis model with an 80 km horizontal resolution (Dee et al. 2011), is used in Sections 3d and 3e to look at the synoptic conditions associated with variations in water isotopes.

In Section 3f, the propensity of deposited snow to retain the sub-monthly isotopic signal observed in precipitation is assessed using annual layer isotopic profiles from snowpit samples collected on four high Andean glaciers in July 2017 (Quelccaya, Illimani, Huayna Potosí and Ancohuma; Fig. 1; Table 2). The sampling frequency was every 8 mm of liquid water equivalent (LWE) at Quelccaya and every 10 mm LWE at the other locations. A visible dust horizon and ice layer signified the base of each annual layer. On Huayna Potosí we were unable to collect samples in the lowest 0.2 m of the annual layer (corresponding to the earliest part of the 2017 wet season) due to time constraints. Daily precipitation measurements scaled to match the total LWE in the snowpit can act as an approximate age model for the annual layer snowpits, allowing for comparison with the average regional isotope signal observed in precipitation. To develop age models for the Quelccaya and Huayna Potosí snowpits we used daily totals of precipitation obtained from an automated precipitation monitoring stations on Quelccaya and Chacaltaya (10 km south-east of Huayna Potosí) respectively. Both of these stations are operated by Appalachian State University. This simple technique to develop an age model assumes no loss of precipitation by sublimation or wind scour during the peak of the wet season.

4. Results

a. d-Excess

The relationship between δD and δ^{18}O is very close to the GMWL for most of the samples at all sites (Fig. 3). We do not observe a significant difference in d-excess values between Austral winter (JJA) compared to Austral summer (DJF), although with only 33 samples from JJA and 780 samples from DJF, our dataset is strongly biased towards the wet season. The highest d-excess values observed ($>$30 ‰) mostly occur during the peak of the wet season and are associated with precipitation that is highly depleted in δ^{18}O. These high d-excess values do not appear to relate to elevation or changes in moisture source region. Over several multiday periods, high d-excess is observed at certain stations in the Cordillera Vilcanota (for example Pucarumi and Sallayoc) but not at others that are only 25 km away (i.e. Murmurani, Chillca). This suggests that these high d-excess values may result from local effects. Because all sites exhibit a strong linear relationship between δ^{18}O and δD, the rest of the analysis focuses on δ^{18}O.

b. Overview of Precipitation Samples

Each year, there is a gradual depletion of ^{18}O in precipitation during the onset of the wet season and enrichment at the onset of the dry season. On a subseasonal basis, there is high variability in δ^{18}O with large amplitude oscillations ($>$ 10 ‰) at individual sites over 1-7 day periods (Fig. 4). In addition, there are cycles of enrichment and depletion that occur approximately every 10-40 days. Sub-monthly δ^{18}O trends exhibit strong synchronicity at all sites, this is particularly apparent in 2017, where there are a large number of stations that cover more than 500 km over land and more than 1500 m in elevation. The range of δ^{18}O values in the first three years (-30 ‰ to +5 ‰) is typical of the range of δ^{18}O values reported in previous studies from this region. However in 2017, there are more significantly depleted events including several samples from multiple sites with δ^{18}O $<$ -35 ‰. The annually averaged δ^{18}O in precipitation in 2016 is 5.6 ‰ higher than the average of the other three years, coinciding with an exceptionally strong El Niño (with a peak Mean ENSO Index of 2.536, Wolter 1993).

c. Spatial Variability

Despite a 1700 m difference in elevation between the highest and lowest sites, there no relationship between elevation and precipitation weighted δ^{18}O or elevation and mean precipitation for the sites summarized in Table 1. There is also no relationship between mean precipitation and δ^{18}O. Mean δ^{18}O varies between sites by just 4.7 ‰ and standard deviation by just 1.04 ‰ suggesting a high degree of agreement between each site despite the differences in elevation and horizontal separation. There are strong, statistically significant ($p < 0.01$) correlations in δ^{18}O between every site (Table 3). Particularly noteworthy is the consistency of the correlation coefficients among sites within the Cordillera Vilcanota and between the Cordillera Vilcanota and the Cordillera Real. This result clearly demonstrates that subseasonal variations of water isotopes in precipitation are integrating a synoptic scale signal and that local effects are of lesser importance, at least not on timescales longer than 3 days.

d. A Regionally Coherent Subseasonal Signal

This section focuses on determining the synoptic conditions that are driving these regionally coherent subseasonal variations by isolating the signal of interest. First, a region-wide isotopic signal is calculated by taking the 3-day precipitation weighted mean δ^{18}O between all sites that provided samples in 2017 (Fig. 5a, black line). Because the number of individual sites collecting a sample on each day varies, the 'average between sites' is sometimes calculated from just one site and sometimes from all seven, however because there is such a good agreement between δ^{18}O at all sites, this does not appear to affect the results.

There are three key modes of temporal variability in this signal. The first, characterized by gradual depletion during the onset of the wet season and enrichment in May and June, is the seasonal cycle. A 90-day moving-average of the mean signal serves to isolate the seasonal cycle (Fig. 5a, orange line). The second mode of variability consists of cycles of relatively more depleted and relatively more enriched periods overlaid on the seasonal cycle that last between 10 and 40 days. A moving average over a period of 15 days captured this observed variability well (Fig. 5a, lime-coloured line), the rest of this study will refer to this signal as the subseasonal signal. Incidentally, 15 days is consistent with the timescale of known variations between wet and dry episodes during the wet season on the Altiplano. The remaining variability captured by the 3-day averaging window relates to short term 'storm scale' oscillations in δ^{18}O, although these variations could record an interesting meteorological signal, it is likely that post-depositional processes will smooth out this signal in the snowpack (see Section 4f.) For this reason, the rest of this study focuses on the subseasonal (15-day moving average) signal.

Subtracting the seasonal cycle from the 15-day moving average isolates the subseasonal signal, yielding a time series of subseasonal δ^{18}O anomalies (Fig. 5b). We characterize negative (more depleted) δ^{18}O anomalies as occasions when the δ^{18}O anomaly is below the 25th percentile for more than 5 days, and positive (more enriched) δ^{18}O anomalies as occasions where the δ^{18}O anomaly is above the 75th percentile for more than 5 days (see Fig 5b). For the remainder of this study, the following naming convention refers to individual subseasonal δ^{18}O anomalies: ±N_YYYY, where N is a sequential number indicating the position of the anomaly (i.e. N=1 is the first anomaly in that year) and YYYY is the year. For example -1_2017 refers to the first negative anomaly during the 2017 wet season that took place between 28 December 2016 and 11 January 2017.

The spatiotemporal consistency of δ^{18}O across the observational domain suggests that regionally coherent meteorological conditions produce these anomalies. Therefore, to identify the key meteorological variables associated with this signal we used data from Era-Interim averaged over the region 12° to 18.5° S and 65° to 74° W (Fig. 2). Five different variables from ERA-Interim

(Table 4) at 250 and 500 hPa were processed in same way as the δ^{18}O time series, by calculating 15-day moving averages and subtracting the seasonal cycle to reveal subseasonal anomalies. The strongest correlations are between δ^{18}O and 500 hPa cloud cover and relative humidity, and 250 hPa zonal wind (Table 4).

Spatially, the positive (negative) δ^{18}O anomalies appear to occur when the Bolivian high is in a more northerly (southerly) position, upper level easterlies are weakened (strengthened) and 500 hPa relative humidity and cloud cover fraction are reduced (increased) over the entire Altiplano and western Amazon basin (Fig. 6a-d). However, comparing the time series of 250 hPa zonal wind anomalies to the δ^{18}O anomalies shows that this signal does not explain all of the δ^{18}O oscillations (Fig. 7c). In particular, -3_2017 does not coincide with a strengthening of the upper level easterlies. During this event, there are also weaker 500 hPa relative humidity and cloud fraction anomalies (Fig. 7a,b), suggesting that -3_2017 was different in nature to -1_2017 and -2_2017. The weaker relative humidity and cloud fraction anomalies might correspond to more localized storms, perhaps restricted to the eastern Cordilleras. Interestingly, most of the high d-excess samples are from -3_2017. There is also a relationship between subseasonal δ^{18}O anomalies and the SALLJ. The positive (negative) δ^{18}O anomalies occur in association with a weakened (strengthened) SALLJ (Fig. 6e,f).

Preceding -1_2017, there is a strong SALLJ and a southward displacement of the Bolivian high resulting in strong upper level easterlies over the study area. During the most depleted period, the SALLJ is at its strongest. After the most depleted period, the SALLJ weakens but the Bolivian high remains in its southward position (Appendix A, Fig. A1). -2_2017 also features a southward displacement of the Bolivian High and enhanced upper level easterly winds before, during and after the event (Appendix A, Fig. A2). Before the event, the SALLJ is much weaker. During the event, the SALLJ strengthens considerably and the 500 hPa winds over the study region switch from easterly to north-westerly. After the event the SALLJ weakens again and the 500 hPa winds return to easterly. The third negative anomaly, -3_2017, (Appendix A, Fig. A3) is the one that is not associated with a strengthening of the upper-level easterly flow. In this case, the Bolivian high is at a similar latitude to the Cordillera Vilcanota throughout the event. Before this event there is a weakening and reversal in the SALLJ north of Santa Cruz, this period coincides with the relatively more enriched precipitation between 7 March and 19 March. During the event the SALLJ strengthens again and remains strong after the event. However, after the event, there is a reduction in the 500 hPa relative humidity over the western Amazon basin.

Before +1_2017 (Appendix A, Fig. A4) the Bolivian high is in an easterly position, the upper level 250 hPa winds are northerly and the SALLJ is weak. During +1_2017, the Bolivian high migrates west and strengthens; the SALLJ weakens further and strong southerly winds over the study area at 500 hPa transport dry air (low relative humidity) to the western Amazon basin. After +1_2017, the Bolivian high weakens, the SALLJ strengthens, the 500 hPa winds weaken and 500 hPa relative humidity in the western Amazon basin begins to increase. Preceding +2_2017 (Appendix A, Fig. A5), an extra-tropical trough extends into southern Bolivia resulting in low 250 hPa geopotential heights. This is associated with a weakening and reversal of the SALLJ and the advection of dry air at 500 hPa into the western Amazon basin by strong southerly winds: we interpret this as a cold air incursion. Following the frontal passage, the SALLJ strengthens considerably during +2_2017, however, dry air remains over the western Amazon basin limiting moisture availability. After +2_2017, the Bolivian high shifts south and the 500 hPa relative humidity begins to increase. Before +3_2017 (Appendix A, Fig. A6) the Bolivian high is displaced to the north and the SALLJ is very weak. During +3_2017, a region of lower 250 hPa geopotential height tracks northward and although the SALLJ appears to strengthen slightly, 500 hPa winds over the study area weaken and there is a reduction in 500 hPa relative humidity in the western Amazon basin. After +3_2017 the SALLJ and the 500 hPa north westerlies return to a more climatological state.

To summarize this section of results, the position of the Bolivian high does not appear to be a consistent factor affecting subseasonal variations in δ^{18}O. Instead, region-wide precipitation events associated very depleted δ^{18}O appear to require both sufficient moisture in the lowlands directly to the east of the Altiplano and a strong SALLJ. These conditions are usually, but not exclusively, associated with a southward displacement of the Bolivian High and strong upper level easterlies. Isotopically enriched precipitation occurs during periods when there is a reduction in regionally averaged cloud cover and relative humidity, associated with either a weakening or reversal of the SALLJ or by a lack of mid-level moisture availability over the western Amazon basin.

It is now possible to test if this result is consistent on an interannual basis by repeating this analysis for the preceding three years using the daily measurements of isotopes in precipitation in the Cordillera Vilcanota. In each year, subseasonal δ^{18}O anomalies occur on similar timescales, although the magnitude of the anomalies vary. Each year the negative δ^{18}O anomalies coincide with a strengthening of the SALLJ and the positive δ^{18}O anomalies are associated with a weakened SALLJ and reduced moisture availability (lower 500 hPa relative humidity) in the Amazon basin to the east of the Altiplano (Fig. 8), demonstrating that this is indeed a robust signal.

e. Relationship with Continental Scale Precipitation Variability

To our knowledge, the only other study that has investigated the controls on stable water isotopes in precipitation in this region using storm-scale sampling over an entire season (1999-2000 hydrological year) is Vimeux et al. (2011). Vimeux et al. (2011) look at the controls on intraseasonal δD variability from several stations in the Zongo valley which passes between our current study sites Chacaltaya and Huayna Potosí in the Cordillera Real. This section tests to see if our data supports the findings of their study, if they apply to the wider region including the Cordillera Vilcanota, and if they are consistent over a multi-year period. In particular, Vimeux et al. (2011) find that the intraseasonal variations in δD in the Zongo valley reflect a continental precipitation dipole related to the position of the SACZ, whereby more enriched (depleted) precipitation in the Zongo valley coincides with enhanced (reduced) convection over north-eastern Brazil and reduced (enhanced) convection over the subtropical plains.

Here we use 500 hPa relative humidity in place of out-going longwave radiation (OLR) because recent studies have demonstrated that much of the precipitation in the tropical Andes is stratiform in nature (Perry et al. 2014, 2017) and therefore OLR is not a good proxy for precipitation amount in this region. 500 hPa relative humidity is strongly correlated with both 500 hPa and 700 hPa cloud cover, and satellite precipitation estimates (not shown) and captures the SACZ dipole.

For each year sampled, there is a positive correlation between the δ^{18}O anomaly signal and detrended 500 hPa relative humidity over the north-eastern Brazil (Fig. 9). Each year there are negative correlations between the δ^{18}O anomaly signal and detrended 500 hPa relative humidity over the tropical Andean region and these extend south-eastwards across the sub-tropical plains in 2015-2017. The strongest correlations with both dipole phases occur during 2016 (the El Niño year, Fig. 9c).

f. Retention of the Region-Wide Subseasonal Isotopic Signal in Annual Layer Snowpits

The previous section demonstrated that subseasonal variations in precipitation δ^{18}O in the Cordilleras Vilcanota and Real are recording changes in synoptic conditions. To use this information in ice core studies, we need to know if seasonal snowpacks retain signals observed in precipitation. There are several ways that the isotopic signal precipitation might be modified or lost in the snow: wind scour or sublimation, meltwater percolation or smoothing of the isotopic signal by molecular diffusion. Each isotopic profile from the four annual layer snowpits sampled in 2017 (see Section 2) featured three prominent δ^{18}O minima that conceivably result from the three negative δ^{18}O anomalies observed in precipitation across the study area. This provides evidence that the snow and ice on these mountains are recording a regionally coherent signal.

When the regional δ^{18}O signal from precipitation is compared to the δ^{18}O profile in the snowpits sampled on Quelccaya and Huayna Potosí, there is excellent pattern matching between the precipitation and the snowpit signals (Fig. 10). On Quelccaya, the best agreement between the two signals occurs when the first 0.25 m of precipitation that fell on Quelccaya is not included in the snowpit; it is conceivable that this early season precipitation was lost via ablation. Because we were not able to sample the lowest 0.2 m of the annual layer snowpack on Huayna Potosí, the early wet season precipitation is not included in this profile. There is a good match between the 15-day moving average isotope signal in precipitation, scaled to precipitation amount at Chacaltaya, when we assume that the first 0.4 m of liquid water equivalent is not included in the snowpit profile due to a combination of early season ablation and the snow that we were unable to sample. The fit to the Huayna Potosí profile is not as good as the fit to the Quelccaya profile, this likely results from the fact that precipitation recorded at Chacaltaya is not completely representative of the precipitation accumulation on Huayna Potosí. Both snowpit signals are slightly more depleted than the precipitation signal (the average snowpit δ^{18}O is 3‰ lower than the average δ^{18}O from precipitation); this could be due to the fact that the precipitation signal is averaged over sites that typically receive liquid precipitation. Solid precipitation (falling at Quelccaya and Huayna Potosí) is typically more depleted (Jouzel and Merlivat 1984). At the top of the snowpit the snowpit profile becomes more enriched than the precipitation, this is likely due to surface enrichment by evaporation at the beginning of the dry season. Plots of the isotopic profiles from Ancohuma and Illimani are not examined here because there were no daily measurements of precipitation that we considered representative of the precipitation that fell on these two mountains. Nevertheless, three highly depleted layers also occur in both of these snowpits (not shown), implying that it would be possible to create accurate age models for these snowpits from precipitation δ^{18}O as well.

5. Discussion

a. δ^{18}O Characteristics in the Cordilleras Vilcanota and Real.

The range of δ^{18}O each year in this study is similar to the range of δ^{18}O identified by previous studies in this region (e.g., Gonfiantini et al. 2001; Fiorella et al. 2015) with the exception of some highly depleted events (δ^{18}O $<$ -35 ‰) that occurred during 2017. The mean annual δ^{18}O each year is similar, except during the strong El Niño year (2015-2016). During this year, there was a severe reduction in snow accumulation on Quelccaya and an enrichment of annually averaged

$\delta^{18}O$ in the annual layer snowpack by 5.2 ‰ (Thompson et al. 2017). The results presented here are consistent with this finding; the average $\delta^{18}O$ in precipitation during 2016 is 5.6 ‰ higher than the average of the other three years. This establishes that the change in $\delta^{18}O$ in the snowpack on Quelccaya resulted from more enriched precipitation rather than post-depositional processes. Despite this, we still observe subseasonal variations in $\delta^{18}O$ that occur on a similar timescales to the other years, suggesting that the El Niño event affected the baseline isotopic content of precipitation as described by previous studies (e.g., Vuille et al. 2003), but that the processes driving the subseasonal variability are the same. Additional years of daily measurements of water isotopes in precipitation covering multiple ENSO events are required to confirm this relationship.

The observations used in this study do not identify a relationship between $\delta^{18}O$ and elevation across our observation sites. This result is in contrast to observations from previous studies in this area of the Andes (Gonfiantini et al. 2001; Vimeux et al. 2005, 2011; Fiorella et al. 2015). However, each of these previous studies have included stations at much lower elevations than the stations used in this study and have not included stations above 4800 m. There is evidence that the 'altitude effect' diminishes at higher altitudes on the Altiplano (Fiorella et al. 2015), and the present study supports this assertion.

On an intraseasonal basis, we visually identify three key modes of variability: the seasonal cycle (90-day moving average), subseasonal oscillations between more enriched and more depleted $\delta^{18}O$ (15-day moving average) and high amplitude short-term variations in $\delta^{18}O$ that occur over periods of 1-7 days. This is consistent with the findings of Vimeux et al. (2011) who identify significant periods of oscillations at 18, 11 and 6 days, and with Hurley et al. (2016) who identify similar intraseasonal periodicities in $\delta^{18}O$ profiles from eight annual layer snowpits on Quelccaya.

Vimeux et al. (2011) also identify a significant mode of variability at 41 days; this was not assessed in the present study. Together these results suggest that the subseasonal δ^{18}O variations that we focus on for the majority of this study are a robust feature retained in annual layer snowpacks.

b. Spatial Coherency

Vimeux et al. (2011) showed that the intraseasonal variability of δD in precipitation was highly coherent between eight sites in the Zongo Valley (Cordillera Real), despite large differences in local precipitation. They interpreted this result as evidence that the precipitation was originating from the same air mass, advected along the valley. The results of the present study support this conclusion and show that the intraseasonal variability is regionally coherent not just in the Zongo valley, but across all of our observation sites in both the Cordilleras Real and Vilcanota. This result has important implications for paleoclimate studies because it demonstrates that the isotopic signals in precipitation that are ultimately preserved in glacial ice have common controls and therefore the isotopic profiles from ice cores extracted from Quelccaya and from Illimani for example can be compared.

c. Relationship with Synoptic Conditions

The excellent spatial matching between the subseasonal δ^{18}O signals at all locations implies that this signal is reflecting synoptic scale rather than local conditions. Strong negative correlations between δ^{18}O and 500 hPa cloud cover, 500 hPa relative humidity and 250 hPa zonal winds all suggest that this variability is reflecting variations in precipitation amount in association with the well documented 'amount effect' (e.g., Dansgaard 1964, Rozanski et al. 1993, Risi et al. 2008). However, physically, the 'amount effect' is caused by a combination of processes and depends on cloud micro-physical processes and precipitation history among other things (see Section 2a). Because the synoptic set up that results in precipitation anomalies over the study area is not the same for each positive or each negative δ^{18}O anomaly (Fig. A1-A6), interpreting positive and negative δ^{18}O anomalies as the regional 'amount effect' alone is likely to have large uncertainties. Of more use to improving paleoclimate reconstructions from ice cores would be to relate the positive and negative δ^{18}O anomalies to the specific synoptic weather systems that are associated with these precipitation anomalies, and the attendant continental scale modes of intraseasonal variability.

Lenters and Cook (1999) describe three synoptic set-ups that can result in positive precipitation anomalies on the Altiplano: a) propagating extra-tropical cyclones that result in a strengthening of the SALLJ, b) a westerly shift of the SACZ and anomalous high pressure over the central Amazon basin forcing a strengthening and southwards shift of the Bolivian High and c) deep narrow bands of low pressure from the subtropics extending into tropical regions along the eastern slopes of the Andes associated with cold air incursions. Considering the individual negative anomaly events from 2017, the -1_2017 and -2_2017 appear to relate to mechanism b), the SACZ shifts to a more westerly position and the Bolivian High is shifted southwards. However -3_2017 appears to relate to mechanism a), with lower 250 hPa geopotential heights over the subtropical plains and the Bolivian High retains a more neutral position. This explains why the first two low anomalies are strongly correlated with upper level zonal with but the third is not. The position of the Bolivian High is therefore not sufficient to explain the δ^{18}O anomalies because it responds differently to these three synoptic setups.

There is also evidence for mechanism c), a cold air incursion appears to occur around 28 January 2017, with a narrow band low 250 hPa geopotential height extending into Bolivia and a reversal of the SALLJ. There does appear to be a short-lived period of very depleted precipitation that occurs region-wide during the onset of this event visible in the 3-day precipitation weighted moving average, however this signal is too short to be captured by the 15-day averaging window (Fig. 5). After the frontal passage, strong southerly winds at 500 hPa along the eastern edge of the Andes advect relatively low humidity air to the east of the study region that persists for several days. This period of time coincides with +2_2017 that is the only positive anomaly that does not coincide with a weakening of the SALLJ. A recent study found evidence that snow layers on Quelccaya that are highly depleted in δ^{18}O relate to MCSs that develop ahead of the frontal passage associated with cold air incursions (Hurley et al. 2015). Figure 10 shows that the 15-day signal is what is recorded in the snow pits, and there is no evidence that the short lived depleted period associated with the cold air incursion is retained in the snow on Quelccaya. In contrast to the findings of Hurley et al. (2015), this cold air incursion appears to result in a more enriched layer in the snow on Quelccaya.

All three negative anomalies that occur in 2017 share a common characteristic, a strengthening of the SALLJ in the Amazon basin directly to the east of the study site. This is a a robust feature for all negative anomalies in all years 2014-2017 (Fig. 8) and occurs during each of the different synoptic set ups. Conversely, the majority of positive anomalies are associated with an anomalously weak or absent SALLJ. During those positive anomalies that are not associated with an anomalously weak SALLJ there is reduced relative humidity directly to the east of the Altiplano. This result implies that SALLJ plays a key role in transporting moisture from the western Amazon basin to the study area and, when there is sufficient moisture available, results in the positive relative humidity and cloud cover anomalies that are associated with the negative δ^{18}O anomalies. Indeed, a recent modeling study found evidence that the SALLJ acts to channel Amazon moisture to the study area by strengthening upslope flow along northwest-oriented valleys (such as the Urubamaba and Apurimac valleys) (Junquas et al. 2017). Other studies have identified a relationship between positive precipitation anomalies and the strength of the SALLJ (e.g., Garreaud 1999; Lenters and Cook 1999; Junquas et al. 2017) or negative δ^{18}O anomalies and the strength of the SALLJ (e.g, Vimeux et al. 2011; Insel et al. 2013) although none of these studies have focused on this relationship.

Another way of distinguishing the synoptic set up associated with each δ^{18}O anomaly might be to consider d-excess in more detail. Several of our samples from 2017 had very high (>30‰) d-excess that did not occur at all stations simultaneously and that does not appear to be related to station elevation or moisture source trajectories. Most of these high d-excess values occur during - 3_2017 that appears to be associated with a propagating extra-tropical wave as opposed to a shift of the SACZ. This δ^{18}O anomaly had weaker 500 hPa relative humidity and cloud fraction anomalies compared to the other negative anomalies. A possible reason for this is that this precipitation event was limited in spatial extent. A positive precipitation anomaly with reduced spatial extend is suggestive of deep convection. Localized high d-excess can occur in the presence of deep convective storms as a result of kinetic processes during ice crystal formation (Jouzel and Merlivat 1984). Verifying this hypothesis by investigating this relationship further is outside the scope of this study but is an important area for future research. It is worth noting that Vimeux et al. (2011) also observed such an event in the 2000 season (very depleted δD with high d-excess).

The results of this study are consistent with the findings of Vimeux et al. (2011), which identifies a relationship between the intraseasonal variations of δ^{18}O in the Zongo valley and a continental-scale precipitation dipole associated with the shifting position of the SACZ. This study demonstrates that this relationship holds over a number of different years and applies in the Cordillera Vilcanota as well as the Cordillera Real. This dipole has a period of 15-20 days (Nogués-Paegle and Mo 1997), consistent with the leading mode of intraseasonal variability in δ^{18}O identified by Vimeux et al. (2011) and in this study. The phase of this dipole is potentially related to the Madden Julian Oscillation (Nogués-Paegle and Mo 1997; Paegle et al. 2000; Alvarez et al. 2016), implying that subseasonal variations in isotopes preserved in annual layer snowpits in the Cordilleras Real and Vilcanota might record information about hemispheric tropical climate variability. The phase of this dipole that is negatively correlated to the subseasonal δ^{18}O signal is also characterized by a strengthening of the SALLJ, explaining how this signal is communicated to the study area. However, as described above, propagating extra-tropical waves can also result in a temporary strengthening of the SALLJ. The subseasonal δ^{18}O signal in tropical Andean precipitation is therefore associated with a combination of the shifting position of the SACZ and propagating extratropical waves. Results from the 2017 season suggest that anomalously depleted δ^{18}O events reflecting propagating extratropical waves might be distinguishable by higher d-excess values, however this conjecture is based on just three negative δ^{18}O anomalies, a longer time series of δ^{18}O in precipitation will be required to test this.

Finally, we find no evidence that these changes in δ^{18}O are a result of changes in moisture source region, implying that they occur either due to changing conditions along the moisture inflow trajectory or at the time of precipitation. Several recent studies have identified a relationship between the organization and extent of precipitation events and precipitation δ^{18}O whereby organized widespread precipitation with a large stratiform component is associated with more depleted precipitation compared to localized convective storms that are more enriched (Kurita et al. 2011; Aggarwal et al. 2016). Recent studies of precipitation delivery along the eastern edge of the Altiplano have identified that there are two key modes of precipitation delivery, afternoon convection due to day-time heating and widespread stratiform precipitation events that occur overnight (Perry et al. 2014, 2017; Chavez and Takahashi 2017). It is conceivable that the periods of more enriched precipitation we see throughout the wet season occur during periods where the precipitation is primarily from localized convective storms formed by daytime heating, whereas the depleted precipitation occurs during periods where the nighttime stratiform precipitation makes up a large component of the total precipitation. This hypothesis is consistent with the findings in this study, when 500 hPa relative humidity is high in the lowlands directly to the east of the Andes, overnight MSCs can form and their stratiform region can spread upslope over the eastern Altiplano (via the mechanism described by Chavez and Takahashi (2017), see Section 2.2). When the SALLJ is weaker and relative humidity is reduced, there is not enough moisture for these systems to form and nighttime down-slope winds resulting from preferential cooling might overpower the SALLJ and restrict nighttime moisture transport into the Altiplano along the northwest-oriented valleys. With this reduction in moisture availability, daytime convective storms are likely to remove the remaining moisture from the atmosphere, preventing the formation of nighttime stratiform events. Verifying this hypothesis is outside the scope of this study.

d. Retention of the Subseasonal Signal in Annual Layer Snow

Annual layer snowpits on high glaciers in the Cordillera Real and the Cordillera Vilcanota clearly exhibit the 15-day averaged δ^{18}O signal that is regionally coherent in precipitation (Fig. 10). These annual layer snowpits are effectively recording changes in synoptic conditions to the east of the Altiplano, in particular, changes in the strength and direction of the SALLJ and in moisture availability in the Amazon lowlands directly east of the Altiplano.

In order to apply the results of this study to interpret paleoclimate signals, it is necessary to consider how the processes that act together to generate the signal we observe today might have changed in the past, and how the subseasonal isotopic signal is modified in deep ice. Molecular diffusion during firnification smooths the isotopic signal over time and, in deep ice, even the seasonal isotopic signal cannot be identified (e.g., Ramirez et al. 2003). However, the isotopic profile from the ice core extracted from Quelccaya in 2003 has an excellent annual resolution for the last 1,500 years (Thompson et al. 2006). Although subseasonal isotopic signals are diminished before they are interred in glacial ice (e.g., Thompson et al. 2017), insoluble chemical tracers that record the same climatic variability may remain in place within annual layering. New technologies have made it possible to obtain many more sample points per annual layer than have previously been available, it is possible that future studies could develop sub-annual climate histories from these data. Such data could offer a wealth of new information about how the climate in this region changed in the past, particularly during the Little Ice Age (that began around 1400 A.D.) and how the climate has responded to historical ENSO events.

6. Conclusions

This study demonstrates that subseasonal variations in δ^{18}O in precipitation in the Cordillera Vilcanota and the Cordillera Real are regionally coherent and reflect synoptic variability. Transitions between more isotopically depleted and enriched precipitation superimposed on the seasonal cycle during the wet season occur on a timescale of 10-40 days. This signal is consistent over a multi-year period that includes a strong El Niño year, and is in agreement with a previous study of intraseasonal δ^{18}O in the same region (Vimeux et al. 2011). More depleted (enriched) events are associated with anomalously high (low) 500 hPa relative humidity and cloud cover over the Altiplano region. These oscillations covary with the following factors: 1) propagating extratropical waves and 2) variability in the strength and position of the SACZ. Both of these factors control the moisture that is transported from the western Amazon basin to eastern Cordilleras of the Altiplano by impacting the strength of the SALLJ and the initial relative humidity of the air mass over the eastern Amazon basin. Anomalously low δ^{18}O in precipitation occurs when the SALLJ is strengthened and anomalously high δ^{18}O occurs when the SALLJ is weakened or reversed, or when there is reduced relative humidity in the Amazon basin along the eastern tropical Andes. The relationship between subseasonal δ^{18}O variability and the continental dipole associated with the variability in the position of the SACZ implies that subseasonal δ^{18}O variability encodes information about continental climatic anomalies and may be related to the MJO.

This subseasonal variability is retained in the isotopic profiles of annual layer snowpits on glaciers in both the Cordillera Real and the Cordillera Vilcanota, enabling the development of accurate snowpit age models. Water isotopes retained in annual layer snowpits on high Andean glaciers in this region are therefore regionally coherent and reflect synoptic and continental scale conditions. These results haves implications for improving paleoclimate reconstructions from tropical Andean ice cores and indicate that annual layering in these ice cores can now be assessed for sub-seasonal variability in precipitation delivery and associated circulation anomalies.

Acknowledgments. We would like to thank all participants in our fieldwork and snow pit efforts 2009-17, the University of Arkansas Stable Isotope Lab for analyzing samples, all of our citizen scientist observers in Peru and Bolivia and our University partners at UNSAAC-Cusco and UMSA-La Paz. This work is funded by US National Science Foundation P2C2 Grant AGS 1566450.

APPENDIX

a. Figures A1 - A7: Temporal plots showing the progression of synoptic conditions for each of the 2017 positive and negative $\delta^{18}O$ anomalies.

References

Aceituno, P., and A. Montecinos, 1993: Circulation anomalies associated with dry and wet periods in the South American Altiplano. *Proc. Fourth Int. Conf. on Southern Hemisphere Meteorology*, Amer. Meteor. Soc), 330–331.

Aggarwal, P. K., O. A. Alduchov, K. O. Froehlich, L. J. Araguas-Araguas, N. C. Sturchio, and N. Kurita, 2012: Stable isotopes in global precipitation: A unified interpretation based on atmospheric moisture residence time. *Geophysical Research Letters*, **39 (11)**.

Aggarwal, P. K., K. Fröhlich, K. M. Kulkarni, and L. L. Gourcy, 2004: Stable isotope evidence for moisture sources in the Asian summer monsoon under present and past climate regimes. *Geophysical Research Letters*, **31 (8)**.

Aggarwal, P. K., U. Romatschke, L. Araguas-Araguas, D. Belachew, F. J. Longstaffe, P. Berg, C. Schumacher, and A. Funk, 2016: Proportions of convective and stratiform precipitation revealed in water isotope ratios. *Nature Geoscience*, **9 (8)**, 624.

Alvarez, M. S., C. Vera, G. Kiladis, and B. Liebmann, 2016: Influence of the Madden Julian Oscillation on precipitation and surface air temperature in South America. *Climate dynamics*, **46 (1-2)**, 245–262.

Bradley, R. S., M. Vuille, D. Hardy, and L. Thompson, 2003: Low latitude ice cores record Pacific sea surface temperatures. *Geophysical Research Letters*, **30 (4)**.

Chavez, S. P., and K. Takahashi, 2017: Orographic rainfall hotspots in the Andes-Amazon transition according to the TRMM precipitation radar and in situ data. *Journal of Geophysical Research: Atmospheres*.

Cifelli, R., N. Doesken, P. Kennedy, L. D. Carey, S. A. Rutledge, C. Gimmestad, and T. Depue, 2005: The community collaborative rain, hail, and snow network: Informal education for scientists and citizens. *Bulletin of the American Meteorological Society*, **86 (8)**, 1069–1077.

Coplen, T. B., P. J. Neiman, A. B. White, J. M. Landwehr, F. M. Ralph, and M. D. Dettinger, 2008: Extreme changes in stable hydrogen isotopes and precipitation characteristics in a landfalling Pacific storm. *Geophysical Research Letters*, **35 (21)**.

Dansgaard, W., 1954: The o18-abundance in fresh water. *Geochimica et Cosmochimica Acta*, **6 (5-6)**, 241–260.

Dansgaard, W., 1964: Stable isotopes in precipitation. *Tellus*, **16 (4)**, 436–468.

Dee, D. P., and Coauthors, 2011: The ERA-Interim reanalysis: Configuration and performance of the data assimilation system. *Quarterly Journal of the royal meteorological society*, **137 (656)**, 553–597.

Dinku, T., S. J. Connor, P. Ceccato, and C. F. Ropelewski, 2008: Comparison of global gridded precipitation products over a mountainous region of Africa. *International Journal of Climatology*, **28 (12)**, 1627–1638.

Doesken, N. J., and A. Judson, 1997: *The snow booklet: A guide to the science, climatology, and measurement of snow in the United States*. Colorado State University Publications & Printing.

Egger, J., and Coauthors, 2005: Diurnal circulation of the Bolivian Altiplano. Part I: observations. *Monthly weather review*, **133 (4)**, 911–924.

Field, R. D., D. Jones, and D. P. Brown, 2010: Effects of postcondensation exchange on the isotopic composition of water in the atmosphere. *Journal of Geophysical Research: Atmospheres*, **115 (D24)**.

Fiorella, R. P., C. J. Poulsen, R. S. Pillco Zolá, J. B. Barnes, C. R. Tabor, and T. A. Ehlers, 2015: Spatiotemporal variability of modern precipitation δ^{18}o in the central Andes and implications for paleoclimate and paleoaltimetry estimates. *Journal of Geophysical Research: Atmospheres*, **120 (10)**, 4630–4656.

Friedman, I., L. Machta, and R. Soller, 1962: Water-vapor exchange between a water droplet and its environment. *Journal of Geophysical Research*, **67 (7)**, 2761–2766.

Garreaud, R., 1999: Multiscale analysis of the summertime precipitation over the central Andes. *Monthly Weather Review*, **127 (5)**, 901–921.

Garreaud, R., 2000: Intraseasonal variability of moisture and rainfall over the South American Altiplano. *Monthly Weather Review*, **128 (9)**, 3337–3346.

Garreaud, R., M. Vuille, and A. C. Clement, 2003: The climate of the Altiplano: observed current conditions and mechanisms of past changes. *Palaeogeography, palaeoclimatology, palaeoecology*, **194 (1)**, 5–22.

Garreaud, R., and J. M. Wallace, 1997: The diurnal march of convective cloudiness over the Americas. *Monthly Weather Review*, **125 (12)**, 3157–3171.

Gat, J., and E. Matsui, 1991: Atmospheric water balance in the Amazon Basin: an isotopic evapotranspiration model. *Journal of Geophysical Research: Atmospheres*, **96 (D7)**, 13 179–13 188.

Gat, J. R., 2000: Atmospheric water balancethe isotopic perspective. *Hydrological processes*, **14 (8)**, 1357–1369.

Gonfiantini, R., 1978: Standards for stable isotope measurements in natural compounds. *Nature*, **271 (5645)**, 534–536.

Gonfiantini, R., M.-A. Roche, J.-C. Olivry, J.-C. Fontes, and G. M. Zuppi, 2001: The altitude effect on the isotopic composition of tropical rains. *Chemical Geology*, **181 (1)**, 147–167.

Grootes, P., M. Stuiver, L. Thompson, and E. Mosley-Thompson, 1989: Oxygen isotope changes in tropical ice, Quelccaya, Peru. *Journal of Geophysical Research: Atmospheres*, **94 (D1)**, 1187–1194.

Hardy, D., M. Vuille, and R. Bradley, 2003: Variability of snow accumulation and isotopic composition on Nevado Sajama, Bolivia. *Journal of Geophysical Research: Atmospheres*, **108 (D22)**.

Hoffmann, G., and Coauthors, 2003: Coherent isotope history of Andean ice cores over the last century. *Geophysical Research Letters*, **30 (4)**.

Houze, R., 1993: Cloud dynamics, 573 pp. *San Diego: Academic. Google Scholar*.

Hurley, J., M. Vuille, and D. Hardy, 2016: Forward modeling of δ^{18}o in Andean ice cores. *Geophysical Research Letters*, **43 (15)**, 8178–8188.

Hurley, J. V., M. Vuille, D. R. Hardy, S. J. Burns, and L. G. Thompson, 2015: Cold air incursions, δ18o variability, and monsoon dynamics associated with snow days at Quelccaya Ice cap, Peru. *Journal of Geophysical Research: Atmospheres*, **120 (15)**, 7467–7487.

Insel, N., C. J. Poulsen, C. Sturm, and T. A. Ehlers, 2013: Climate controls on Andean precipitation δ^{18}o interannual variability. *Journal of Geophysical Research: Atmospheres*, **118 (17)**, 9721–9742.

Jouzel, J., and L. Merlivat, 1984: Deuterium and oxygen 18 in precipitation: Modeling of the isotopic effects during snow formation. *Journal of Geophysical Research: Atmospheres*, **89 (D7)**, 11 749–11 757.

Junquas, C., K. Takahashi, T. Condom, J.-C. Espinoza, S. Chavez, J.-E. Sicart, and T. Lebel, 2017: Understanding the influence of orography on the precipitation diurnal cycle and the associated atmospheric processes in the central Andes. *Climate Dynamics*, 1–23.

Kurita, N., 2013: Water isotopic variability in response to mesoscale convective system over the tropical ocean. *Journal of Geophysical Research: Atmospheres*, **118 (18)**.

Kurita, N., D. Noone, C. Risi, G. A. Schmidt, H. Yamada, and K. Yoneyama, 2011: Intraseasonal isotopic variation associated with the Madden-Julian Oscillation. *Journal of Geophysical Research: Atmospheres*, **116 (D24)**.

Lawrence, J. R., and Coauthors, 2004: Stable isotopic composition of water vapor in the tropics. *Journal of Geophysical Research: Atmospheres*, **109 (D6)**.

Lenters, J., and K. Cook, 1997: On the origin of the Bolivian High and related circulation features of the South American climate. *Journal of the Atmospheric Sciences*, **54 (5)**, 656–678.

Lenters, J., and K. Cook, 1999: Summertime precipitation variability over South America: Role of the large-scale circulation. *Monthly Weather Review*, **127 (3)**, 409–431.

Liotta, M., R. Favara, and M. Valenza, 2006: Isotopic composition of the precipitations in the central Mediterranean: Origin marks and orographic precipitation effects. *Journal of Geophysical Research: Atmospheres*, **111 (D19)**.

Marengo, J. A., W. R. Soares, C. Saulo, and M. Nicolini, 2004: Climatology of the low-level jet east of the Andes as derived from the NCEP NCAR reanalyses: Characteristics and temporal variability. *Journal of Climate*, **17**, 2261–2280.

Mayewski, P., S. Sneed, S. Birkel, A. Kurbatov, and K. Maasch, 2014: Holocene warming marked by abrupt onset of longer summers and reduced storm frequency around Greenland. *Journal of Quaternary Science*, **29 (1)**, 99–104.

Nogués-Paegle, J., and K. C. Mo, 1997: Alternating wet and dry conditions over South America during summer. *Monthly Weather Review*, **125 (2)**, 279–291.

Paegle, J. N., L. A. Byerle, and K. C. Mo, 2000: Intraseasonal modulation of South American summer precipitation. *Monthly Weather Review*, **128 (3)**, 837–850.

Perry, L. B., A. Seimon, and G. M. Kelly, 2014: Precipitation delivery in the tropical high Andes of southern Peru: new findings and paleoclimatic implications. *International Journal of Climatology*, **34 (1)**, 197–215.

Perry, L. B., and Coauthors, 2017: Characteristics of precipitating storms in glacierized tropical Andean cordilleras of Peru and Bolivia. *Annals of the American Association of Geographers*, **107 (2)**, 309–322.

Pfahl, S., and H. Sodemann, 2014: What controls deuterium excess in global precipitation? *Climate of the Past*, **10 (2)**, 771.

Rabatel, A., and Coauthors, 2013: Current state of glaciers in the tropical Andes: a multi-century perspective on glacier evolution and climate change. *The Cryosphere*, **7 (1)**, 81.

Ramirez, E., and Coauthors, 2003: A new Andean deep ice core from Nevado Illimani (6350 m), Bolivia. *Earth and Planetary Science Letters*, **212 (3-4)**, 337–350.

Risi, C., S. Bony, and F. Vimeux, 2008: Influence of convective processes on the isotopic composition (δ^{18}o and δd) of precipitation and water vapor in the tropics: 2. Physical interpretation of the amount effect. *Journal of Geophysical Research: Atmospheres*, **113 (D19)**.

Rozanski, K., L. Araguás-Araguás, and R. Gonfiantini, 1993: Isotopic patterns in modern global precipitation. *Climate change in continental isotopic records*, 1–36.

Scheel, M., M. Rohrer, C. Huggel, D. S. Villar, E. Silvestre, and G. Huffman, 2011: Evaluation of TRMM Multi-satellite Precipitation Analysis (TMPA) performance in the Central Andes region and its dependency on spatial and temporal resolution. *Hydrology and Earth System Sciences*, **15 (8)**, 2649.

Stewart, M. K., 1975: Stable isotope fractionation due to evaporation and isotopic exchange of falling waterdrops: Applications to atmospheric processes and evaporation of lakes. *Journal of Geophysical Research*, **80 (9)**, 1133–1146.

Sturm, C., F. Vimeux, and G. Krinner, 2007: Intraseasonal variability in South America recorded in stable water isotopes. *Journal of Geophysical Research: Atmospheres*, **112 (D20)**.

Thompson, L., and Coauthors, 2017: Impacts of recent warming and the 2015/2016 El niño on tropical Peruvian ice fields. *Journal of Geophysical Research: Atmospheres*.

Thompson, L. G., 2000: Ice core evidence for climate change in the Tropics: implications for our future. *Quaternary Science Reviews*, **19 (1)**, 19–35.

Thompson, L. G., E. Mosley-Thompson, M. Davis, V. Zagorodnov, I. Howat, V. Mikhalenko, and P.-N. Lin, 2013: Annually resolved ice core records of tropical climate variability over the past˜ 1800 years. *Science*, **340 (6135)**, 945–950.

Thompson, L. G., and Coauthors, 2006: Abrupt tropical climate change: Past and present. *Proceedings of the National Academy of Sciences*, **103 (28)**, 10 536–10 543.

Vera, C., and Coauthors, 2006: The south american low-level jet experiment. *Bulletin of the American Meteorological Society*, **87 (1)**, 63–77.

Vergara, W., A. Deeb, A. Valencia, R. Bradley, B. Francou, A. Zarzar, A. Grünwaldt, and S. Haeussling, 2007: Economic impacts of rapid glacier retreat in the Andes. *Eos, Transactions American Geophysical Union*, **88 (25)**, 261–264.

Villacís, M., F. Vimeux, and J. D. Taupin, 2008: Analysis of the climate controls on the isotopic composition of precipitation (δ^{18}o) at Nuevo Rocafuerte, 74.5 w, 0.9 s, 250 m, Ecuador. *Comptes Rendus Geoscience*, **340 (1)**, 1–9.

Vimeux, F., R. Gallaire, S. Bony, G. Hoffmann, and J. C. Chiang, 2005: What are the climate controls on δd in precipitation in the Zongo Valley (Bolivia)? implications for the Illimani ice core interpretation. *Earth and Planetary Science Letters*, **240 (2)**, 205–220.

Vimeux, F., P. Ginot, M. Schwikowski, M. Vuille, G. Hoffmann, L. G. Thompson, and U. Schotterer, 2009: Climate variability during the last 1000 years inferred from Andean ice cores: A review of methodology and recent results. *Palaeogeography, Palaeoclimatology, Palaeoecology*, **281 (3)**, 229–241.

Vimeux, F., G. Tremoy, C. Risi, and R. Gallaire, 2011: A strong control of the South American SeeSaw on the intra-seasonal variability of the isotopic composition of precipitation in the Bolivian Andes. *Earth and Planetary Science Letters*, **307 (1)**, 47–58.

Vuille, M., 1999: Atmospheric circulation over the Bolivian Altiplano during dry and wet periods and extreme phases of the Southern Oscillation. *International Journal of Climatology*, **19**, 1579–1600.

Vuille, M., and C. Ammann, 1997: Regional snowfall patterns in the high, arid Andes. *Climatic change*, **36 (3-4)**, 413–423.

Vuille, M., R. Bradley, R. Healy, M. Werner, D. Hardy, L. Thompson, and F. Keimig, 2003: Modeling δ^{18}o in precipitation over the tropical Americas: 2. simulation of the stable isotope signal in Andean ice cores. *Journal of Geophysical Research: Atmospheres*, **108 (D6)**.

Vuille, M., and M. Werner, 2005: Stable isotopes in precipitation recording South American summer monsoon and ENSO variability: observations and model results. *Climate Dynamics*, **25 (4)**, 401–413.

Vuille, M., and Coauthors, 2017: Rapid decline of snow and ice in the tropical Andes–impacts, uncertainties and challenges ahead. *Earth-Science Reviews*.

Wolter, K., 1993: Monitoring ENSO in COADS with a seasonally adjusted principal component index. *Proc. of the 17th Climate Diagnostics Workshop, 1993*.

Zhou, J., and K.-M. Lau, 2001: Principal modes of interannual and decadal variability of summer rainfall over South America. *International Journal of Climatology*, **21 (13)**, 1623–1644.

LIST OF TABLES

Table 1. Characteristics of each of the stations and samples that were collected during the period used to analyze spatial variability (6 December 2016 to 30 April 2017). SD stands for standard deviation. Stations with asterisks are located in the Cordillera Real; all other stations are located in the Cordillera Vilcanota. There is no mean precipitation value for Chillca and Phinaya because these observers did not record non-measurable precipitation events and Chillca did not record most events <5mm. 49

Table 2. Details of annual layer snowpits sampled in 2017. 50

Table 3. Correlation matrix showing Pearson's product moment correlation coefficients between the 3-day precipitation weighted mean δ^{18}O at each station between 6 December 2016 and 30 April 2017. All correlations are significant at the 99% confidence interval or greater 51

Table 4. Correlation matrix showing the Pearson's product moment correlation coefficients between the timeseries of 2017 δ^{18}O anomalies and variables from ERA-Interim reanalysis (15-day moving average minus the subseasonal signal). Variables: r = relative humidity, t = temperature, z = geopotential height, cc = cloud cover fraction, u = zonal wind. The numbers beside each variable refer to the level in the atmosphere (hPa). Correlations that are significant at the at the 99% confidence interval are highlighted with an asterisks. 52

TABLE 1. Characteristics of each of the stations and samples that were collected during the period used to analyze spatial variability (6 December 2016 to 30 April 2017). SD stands for standard deviation. Stations with asterisks are located in the Cordillera Real; all other stations are located in the Cordillera Vilcanota. There is no mean precipitation value for Chillca and Phinaya because these observers did not record non-measurable precipitation events and Chillca did not record most events $<$5mm.

Station	Elevation (masl)	N samples	Mean precipitation (mm d^{-1})	Mean $\delta^{18}O$ (‰)	SD $\delta^{18}O$ (‰)
Murmurani	5050	91	3.10	-20.6	8.72
Phinaya	4750	62	–	-21.9	8.18
Chillca	4250	35	–	-17.5	8.51
Pucarumi	4150	95	5.10	-16.7	6.76
Tuxahuira	3523	90	8.56	-15.9	6.99
Perayoc	3350	65	3.73	-18.0	8.76
Warisata	3350	42	1.92	-19.3	7.53

TABLE 2. Details of annual layer snowpits sampled in 2017.

Location	Date (2017)	Elevation (m)	Depth (m)
Quelccaya	16 July	5620	2.16
Illimani	22 July	6318	1.81
Ancohuma	26 July	5890	1.62
Huayna Potosí	29 July	5913	2.57*

*Annual layer was 2.8 m deep, lowest 0.23 m not sampled

TABLE 3. Correlation matrix showing Pearson's product moment correlation coefficients between the 3-day precipitation weighted mean δ^{18}O at each station between 6 December 2016 and 30 April 2017. All correlations are significant at the 99% confidence interval or greater

	Murmurani	Pucarumi	Perayoc	Phinaya	Chillca	Tuxahuira	Warisata
Murmurani	1	Pucarumi					
Pucarumi	0.61	1	Perayoc				
Perayoc	0.69	0.83	1	Phinaya			
Phinaya	0.67	0.81	0.9	1	Chillca		
Chillca	0.46	0.73	0.77	0.78	1	Tuxahuira	
Tuxahuira	0.69	0.82	0.83	0.82	0.79	1	Warisata
Warisata	0.55	0.68	0.74	0.75	0.82	0.78	1

TABLE 4. Correlation matrix showing the Pearson's product moment correlation coefficients between the timeseries of 2017 δ^{18}O anomalies and variables from ERA-Interim reanalysis (15-day moving average minus the subseasonal signal). Variables: r = relative humidity, t = temperature, z = geopotential height, cc = cloud cover fraction, u = zonal wind. The numbers beside each variable refer to the level in the atmosphere (hPa). Correlations that are significant at the at the 99% confidence interval are highlighted with an asterisks.

	$\delta^{18}O$	r250	r500	t250	t500	z250	z500	cc250	cc500	u250	u500
δ^{18}O	1	r250									
r250	-0.72*	1	r500								
r500	-0.88*	0.74*	1	t250							
t250	-0.51*	0.53*	0.54*	1	t500						
t500	0.17	0.16	-0.21	0.53*	1	z250					
z250	-0.28*	0.44*	0.37*	0.72*	0.67*	1	z500				
z500	0.21	-0.07	-0.11	-0.08	0.25*	0.59*	1	cc250			
cc250	-0.59*	0.73*	0.51*	0.11	-0.19	-0.06	-0.28*	1	cc500		
cc500	-0.74*	0.54*	0.89*	0.49*	-0.26*	0.29*	-0.15	0.33*	1	u250	
u250	0.73*	-0.65*	-0.85*	-0.67*	0.01	-0.38*	0.25*	-0.36*	-0.75*	1	u500
u500	0.02	-0.18	-0.32*	-0.40*	-0.18	-0.46*	-0.27*	0.23	-0.36*	0.55*	1

LIST OF FIGURES

Fig. A1. Temporal progression of synoptic conditions associated with -1_2017 (26 Dec 2016 to 12 Jan 2017). Conditions averaged over the 6 days preceding (A-C), centered on (D-F) and after (G-I) the event. First column (A,D,G): 250 hPa geopotential heights (contoured) and winds. Second column (B,E,H): 850 hPa geopotential heights (contoured) and winds. Third column (C,F,I): 500 hPa relative humidity and winds. The black star shows the location of Quelccaya. 55

Fig. A2. The same as A1 but for -2_2017: 22 Feb 2017 to 7 Mar 2017 56

Fig. A3. The same as A1 but for -3_2017: 19 Mar 2017 to 4 Apr 2017 57

Fig. A4. The same as A1 but for +1_2017: 12 Dec 2016 to 22 Dec 2016 58

Fig. A5. The same as A1 but for +2_2017: 21 Jan 2017 to 14 Feb 2017 59

Fig. A6. The same as A1 but for +3_2017: 12 Apr 2017 to 24 Apr 2017 60

Fig. 1. Study area. Left panel: the locations of the Cordilleras Vilcanota and Real, the four snowpit sampling locations (blue triangles) and the locations of the nearby cities of Cusco and La Paz (white stars). Right panel: key features of South American circulation discussed in this study. SACZ = South Atlantic Convergence Zone, SALLJ = South American Low Level Jet. . 61

Fig. 2. Locations of precipitation collection sites. The table inset lists station names, elevations (meters above sea level) and the start date of each record. 62

Fig. 3. δ^{18}O and δD of each daily precipitation sample used in this study (2014-2017). Different shapes/ colors correspond to different stations (see legend inset). Samples with a d-excess <0‰ and precipitation amount <25 mm are not included (see explanation in section 3). The global meteoric water line is plotted for comparison (black line). 63

Fig. 4. Time series of δ^{18}O in all precipitation samples (2014-2017 = A-D respectively). Samples are plotted from August to August and each year is labeled after the year in which the wet season finishes. Although August does not necessarily reflect the transition between wet and dry seasons, it allows us to focus on the wet season and is sufficient for the purpose of this study. We use this naming convention in the rest of this paper. Samples from different stations are plotted in different colors (see legends inset). Solid lines join samples collected on consecutive days. The dashed blue line marks the average δ^{18}O each year (included in the legend). 64

Fig. 5. A) δ^{18}O of all precipitation samples collected in 2017 (points, see legend inset), 3-day precipitation weighted mean of all samples (solid black line), 15-day moving average of the 30 day signal (dot-dash, green line, referred to as the subseasonal signal in this study) and the 90-day moving average of the 3-day signal (dashed, orange line, referred to as the seasonal cycle in this study). B) Subseasonal δ^{18}O anomalies during the 2017 wet season (subseasonal signal minus the seasonal cycle). Red shading highlights positive (+) anomalies where the δ^{18}O anomaly is above the 75th percentile for at least 5 days and blue shading highlights negative (-) anomalies where the δ^{18}O anomaly is below the 25th percentile for at least 5 days. 65

Fig. 6. Difference between positive and negative δ^{18}O anomalies in 2017. (A) and (B) show 250 hPa geopotential heights (contoured) and winds averaged over all of the positive anomalies and all of the negative anomalies respectively. (C) and (D) are difference plots, showing the average over all positive anomalies minus the average of all negative anomalies for 500 hPa relative humidity and 500 hPa cloud cover respectively. Black dots on the different plots show areas where the difference is significant at the 99% confidence interval. (E) and (F) show 850 hPa geopotential heights (contoured) and winds averaged over all of the positive anomalies and all of the negative anomalies respectively. The black star on each plot shows the location of Quelccaya in the Cordillera Vilcanota. 66

Fig. 7. 2017 time series of anomalies in (A) 500 hPa relative humidity, (B) 500 hPa cloud fraction and (C) 250 hPa zonal wind (solid blue line). Each anomaly series is calculated by subtracting the 90-day moving average (seasonal cycle) from the 15-day moving average of each field from ERA-Interim data averaged over the region 18.5° to 12° S and 74° to 65° W . The time series of δ^{18}O anomalies is overlaid on each plot for comparison (grey dashed line). . . 67

Fig. 8. δ^{18}O anomaly plots for each wet season calculated in the same was as in Fig. 5b: (A) 2014, (D) 2015, (G) 2016. Adjacent to each anomaly plot are spatial plots of 500 hPa relative humidity and 850 hPa winds averaged over each negative anomaly (B,E,H) and each positive anomaly (C,F,I) for each respective year. The black star on each spatial plot shows the location of Quelccaya 68

Fig. 9. Pearson's product-moment correlation coefficients between the time-series of δ^{18}O anomalies and time-series of 500 hPa relative humidity anomalies at every grid-point for each year. Black dots highlight areas where the correlation is significant at the 99% confidence level. On each plot the black star shows the location of Quelccaya. 69

Fig. 10. δ^{18}O profiles of the annual layer snowpits on Quelccaya (A) and Huayna Potosí (B) sampled in July 2017. Overlain on each snowpit profile is the 15-day moving average δ^{18}O signal observed in region-wide precipitation, scaled to the liquid water equivalent depth in each snowpit from precipitation measurements from Quelccaya (A) and Chacaltaya (B), (red dashed line). Blue triangles are plotted every 5 days showing the snowpit age model. Vertical blue lines are plotted on the first day of each month. 70

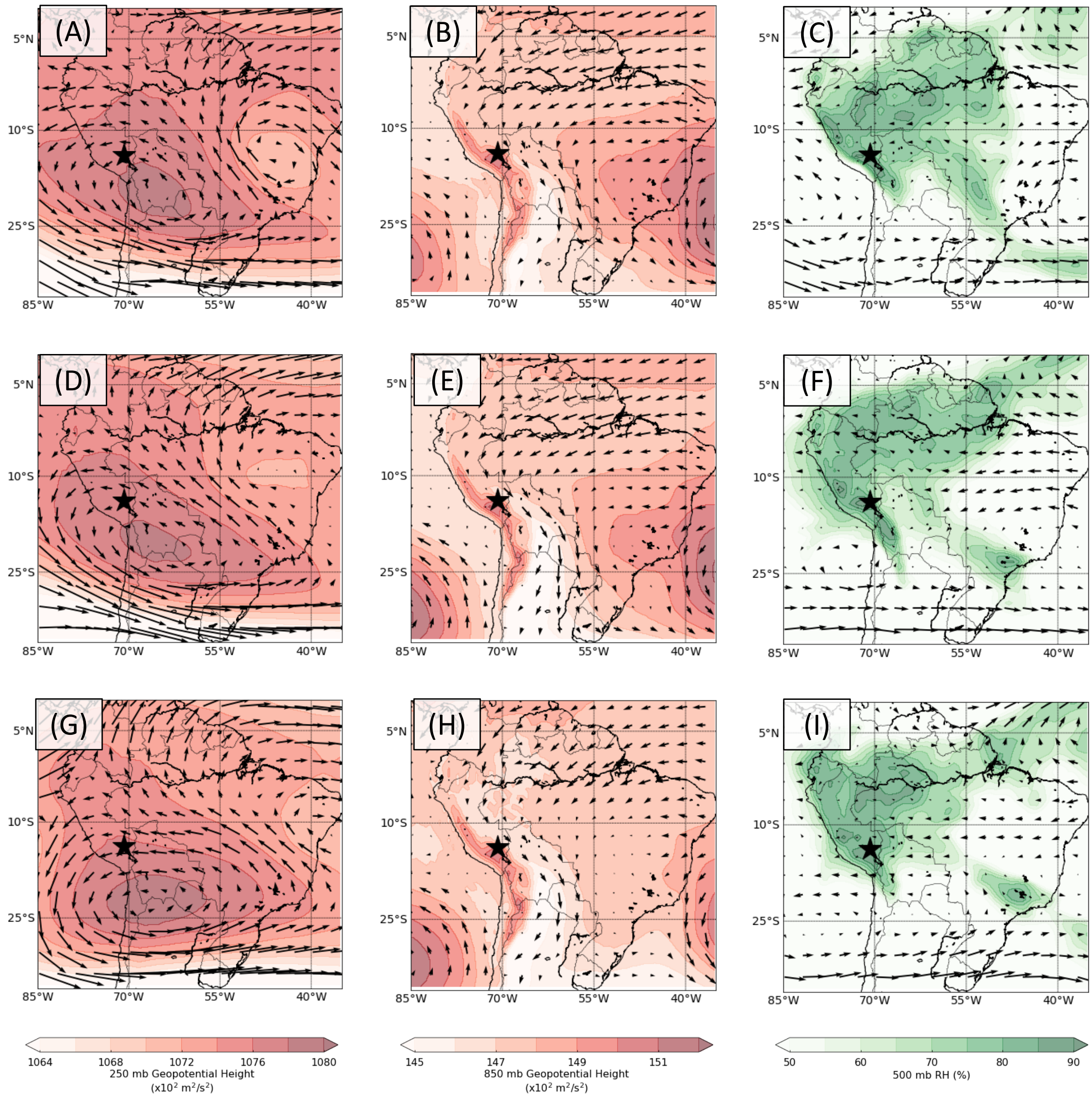

Fig. A1. Temporal progression of synoptic conditions associated with -1_2017 (26 Dec 2016 to 12 Jan 2017). Conditions averaged over the 6 days preceding (A-C), centered on (D-F) and after (G-I) the event. First column (A,D,G): 250 hPa geopotential heights (contoured) and winds. Second column (B,E,H): 850 hPa geopotential heights (contoured) and winds. Third column (C,F,I): 500 hPa relative humidity and winds. The black star shows the location of Quelccaya.

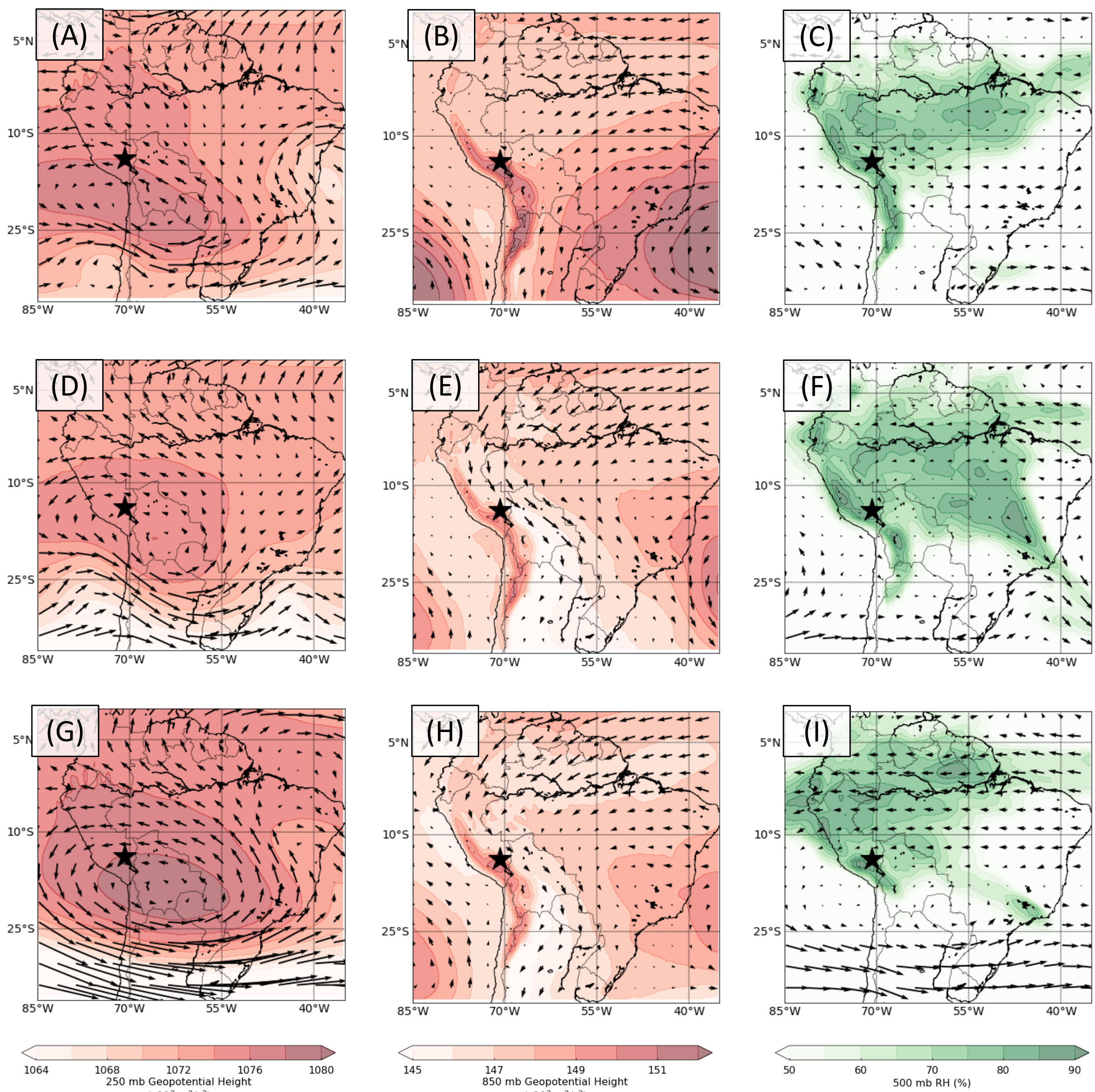

Fig. A2. The same as A1 but for -2_2017: 22 Feb 2017 to 7 Mar 2017

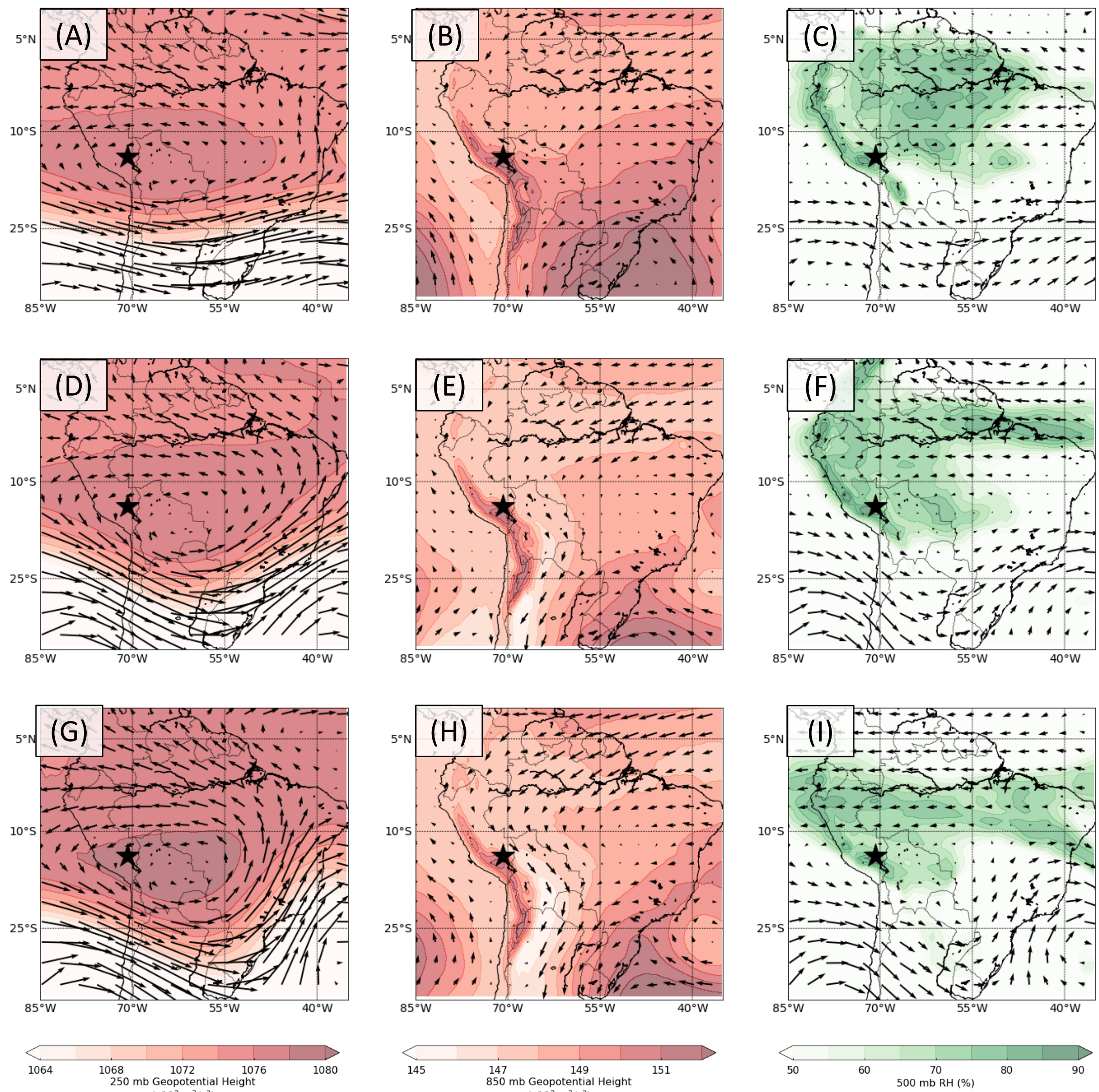

Fig. A3. The same as A1 but for -3_2017: 19 Mar 2017 to 4 Apr 2017

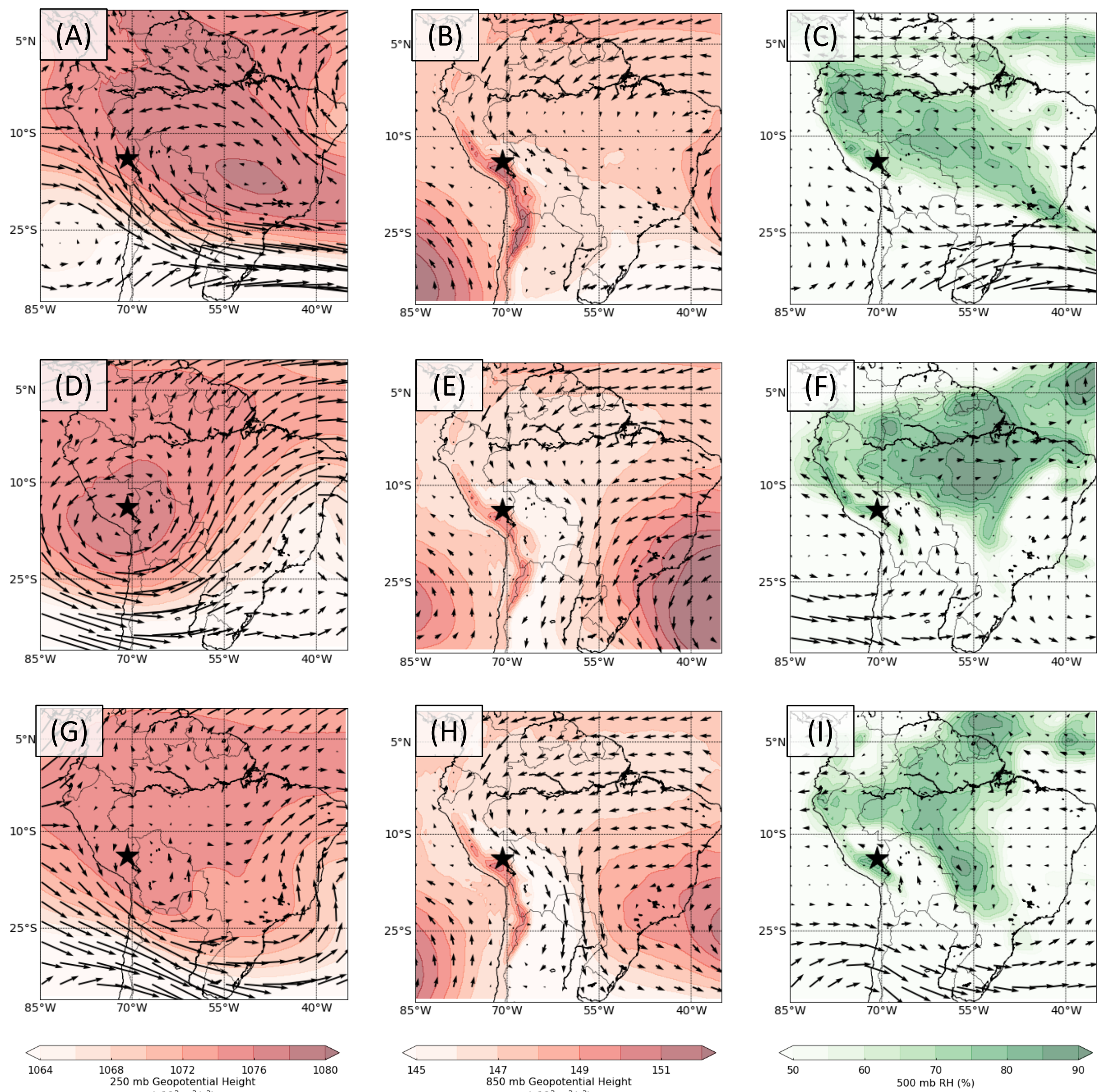

Fig. A4. The same as A1 but for +1_2017: 12 Dec 2016 to 22 Dec 2016

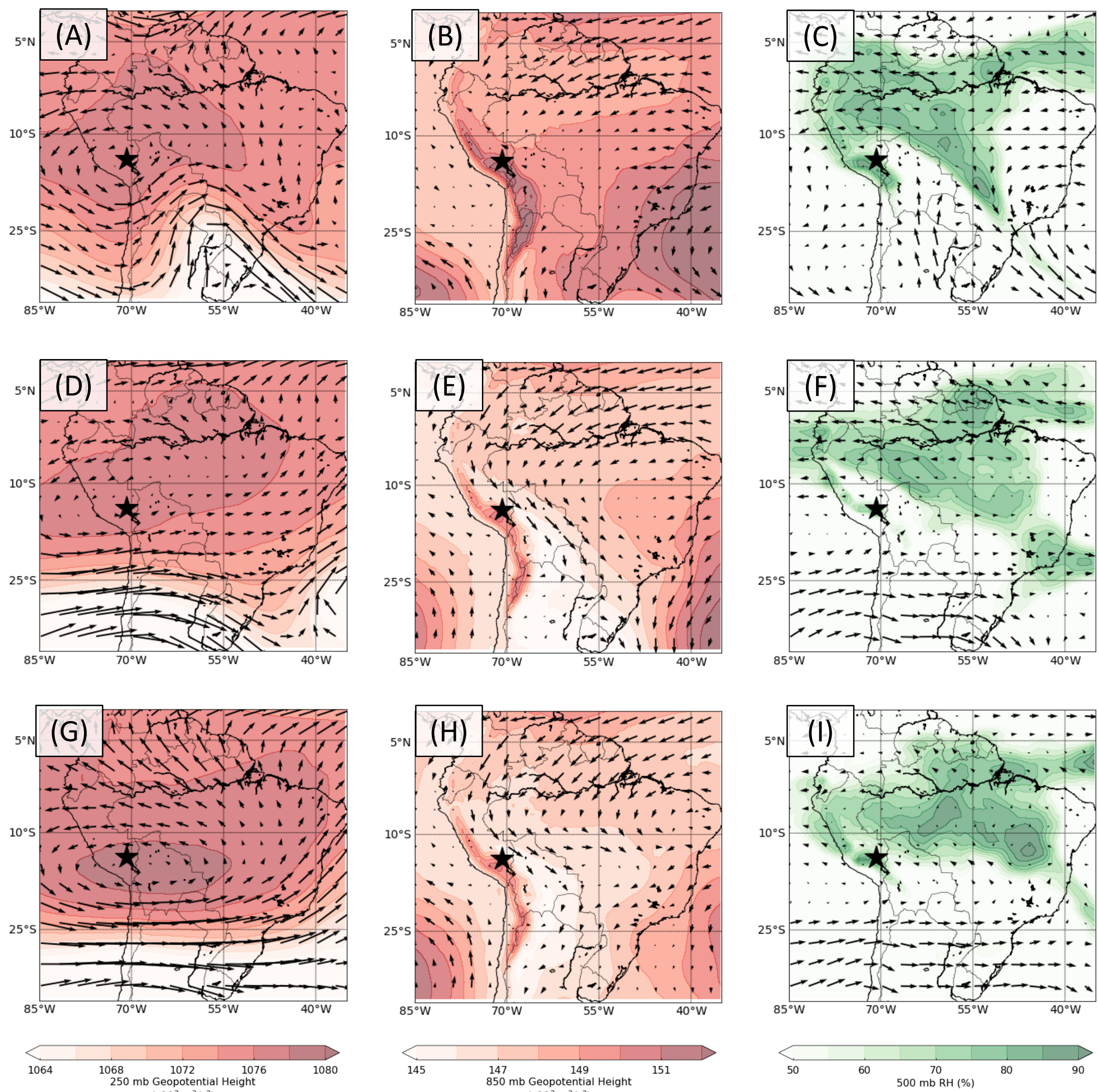

Fig. A5. The same as A1 but for +2_2017: 21 Jan 2017 to 14 Feb 2017

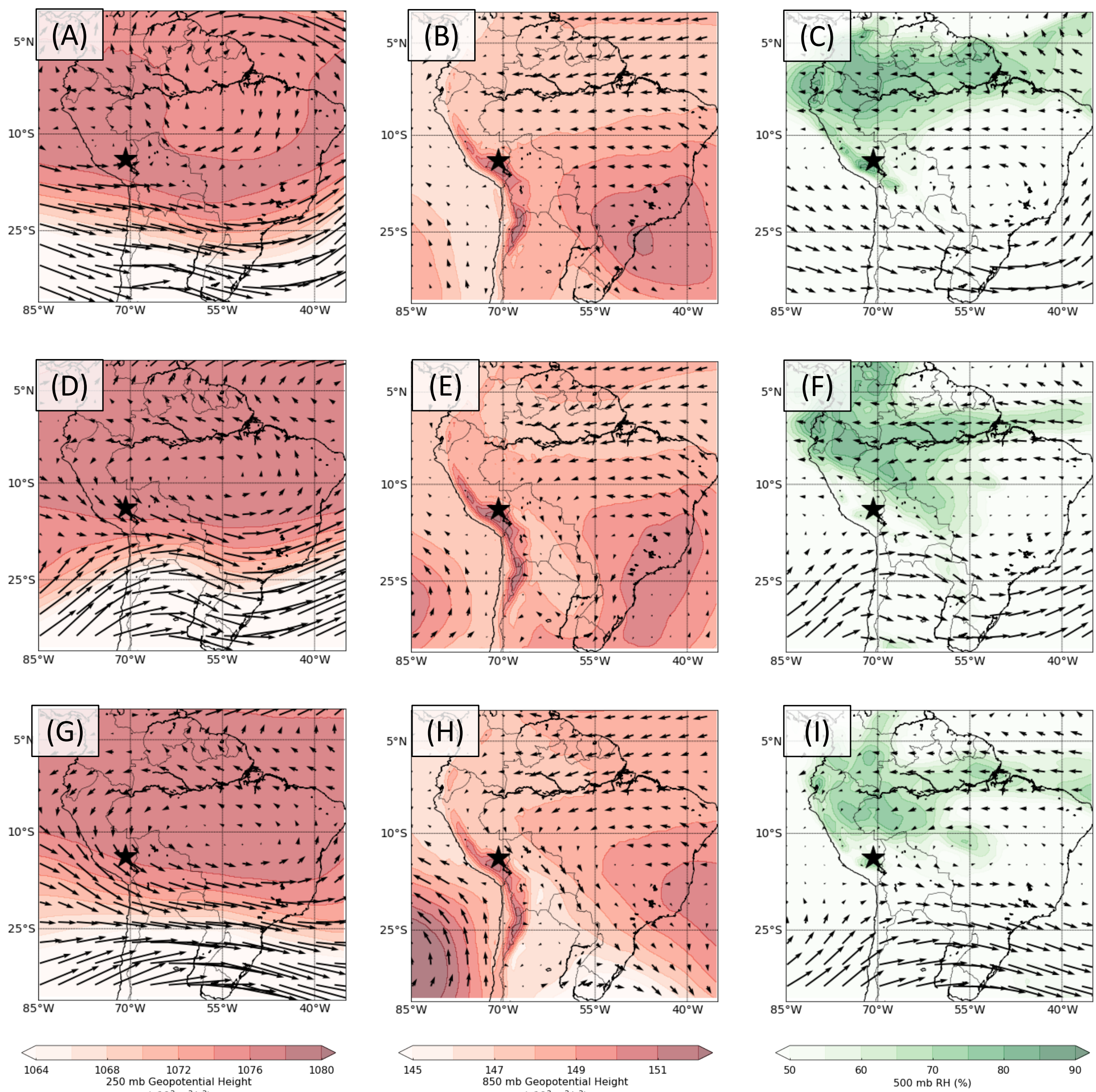

Fig. A6. The same as A1 but for +3_2017: 12 Apr 2017 to 24 Apr 2017

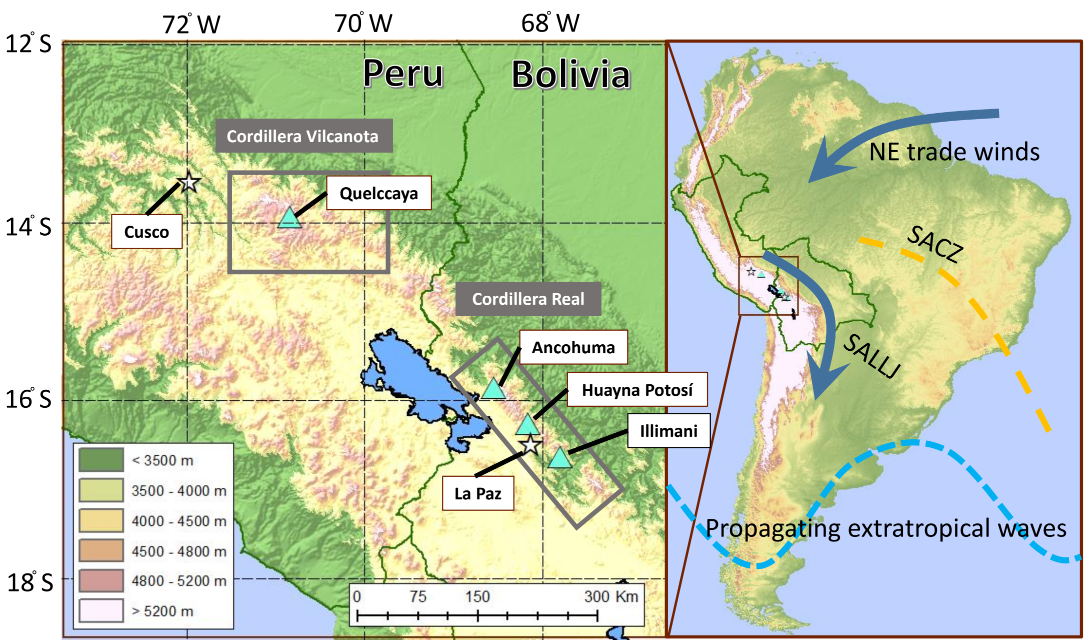

1084 FIG. 1. Study area. Left panel: the locations of the Cordilleras Vilcanota and Real, the four snowpit sampling locations (blue triangles) and the locations of the nearby cities of Cusco and La Paz (white stars). Right panel: key features of South American circulation discussed in this study. SACZ = South Atlantic Convergence Zone, SALLJ = South American Low Level Jet.

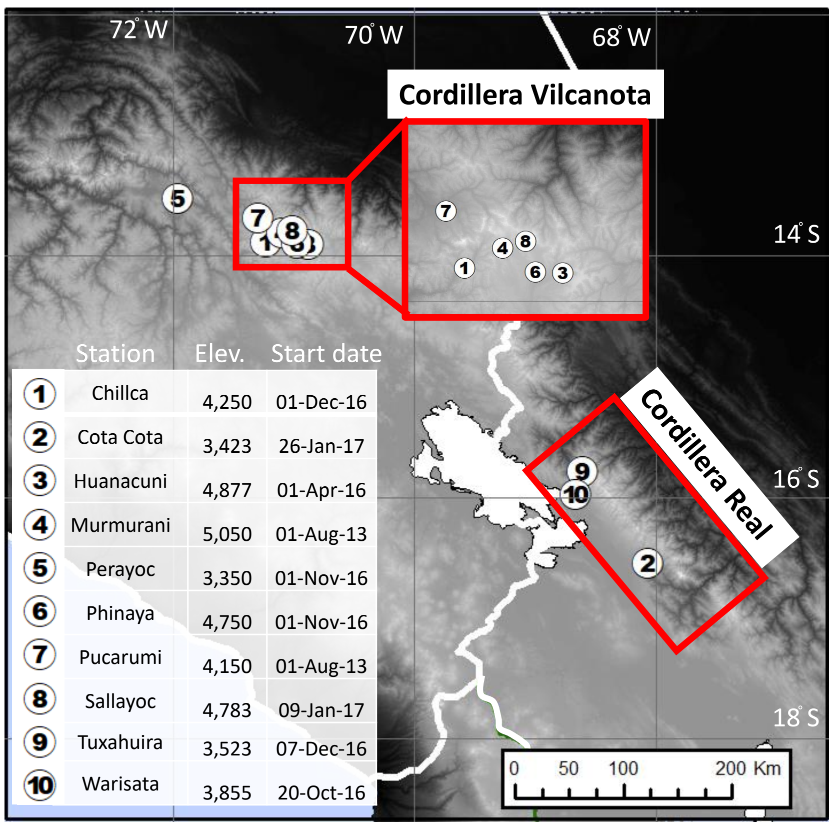

FIG. 2. Locations of precipitation collection sites. The table inset lists station names, elevations (meters above sea level) and the start date of each record.

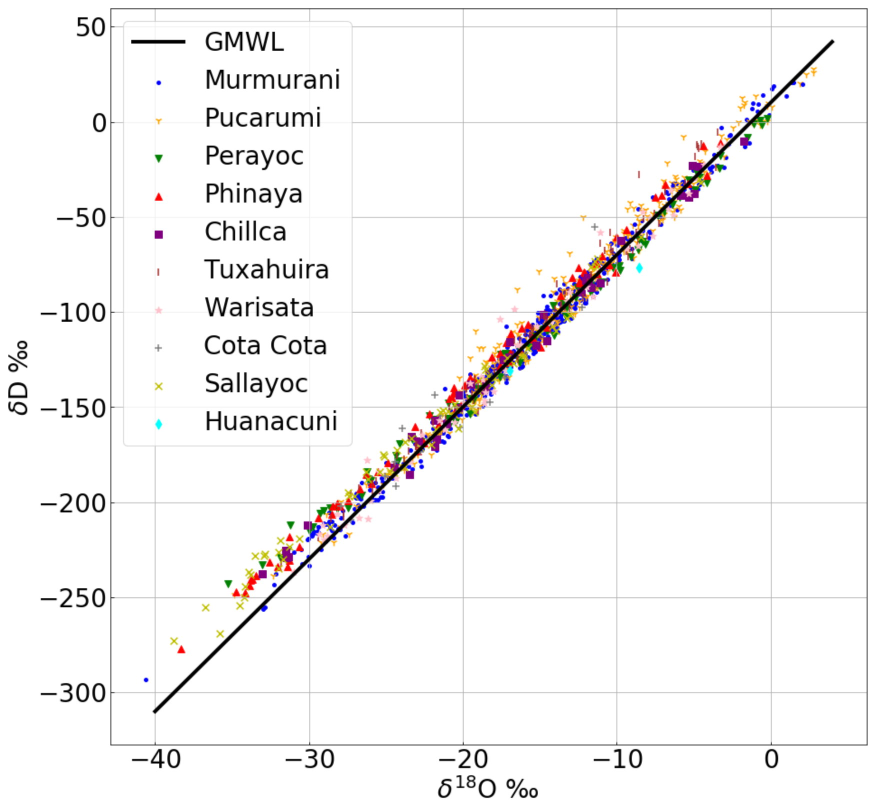

FIG. 3. δ^{18}O and δD of each daily precipitation sample used in this study (2014-2017). Different shapes/ colors correspond to different stations (see legend inset). Samples with a d-excess $<0‰$ and precipitation amount <25 mm are not included (see explanation in section 3). The global meteoric water line is plotted for comparison (black line).

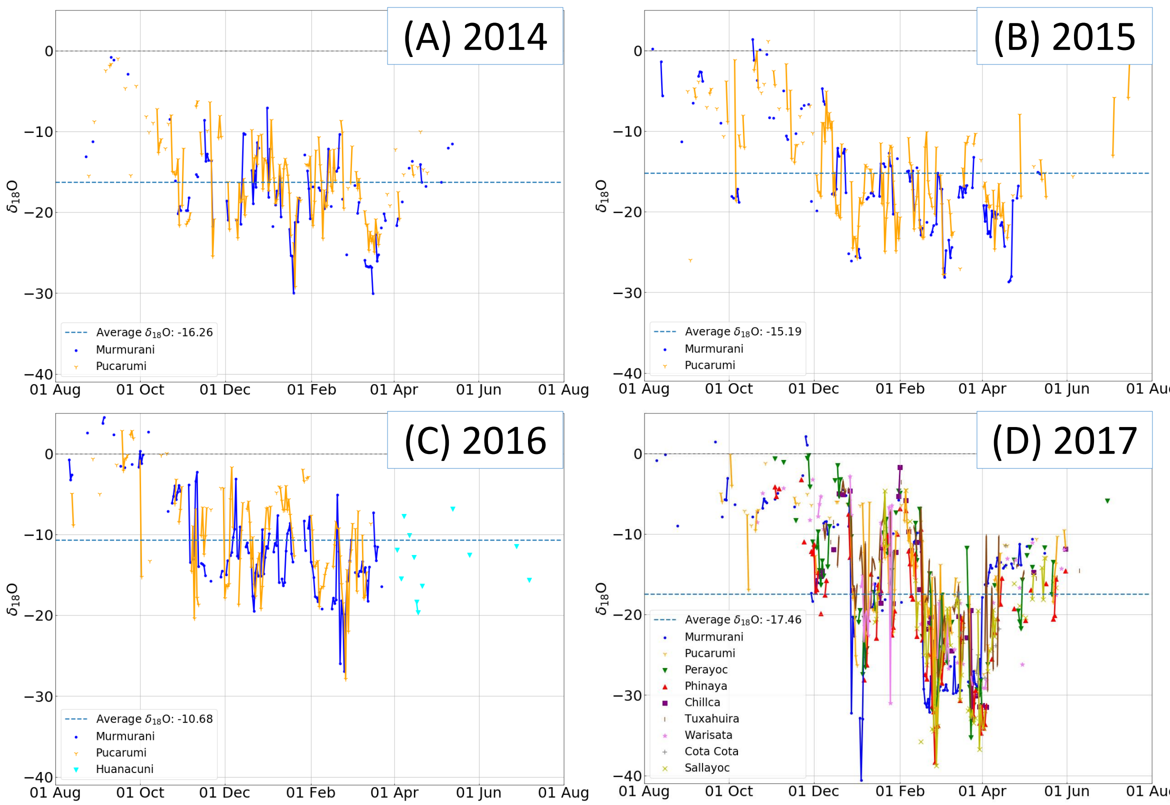

1094 FIG. 4. Time series of δ^{18}O in all precipitation samples (2014-2017 = A-D respectively). Samples are plotted
1095 from August to August and each year is labeled after the year in which the wet season finishes. Although August
1096 does not necessarily reflect the transition between wet and dry seasons, it allows us to focus on the wet season
1097 and is sufficient for the purpose of this study. We use this naming convention in the rest of this paper. Samples
1098 from different stations are plotted in different colors (see legends inset). Solid lines join samples collected on
1099 consecutive days. The dashed blue line marks the average δ^{18}O each year (included in the legend).

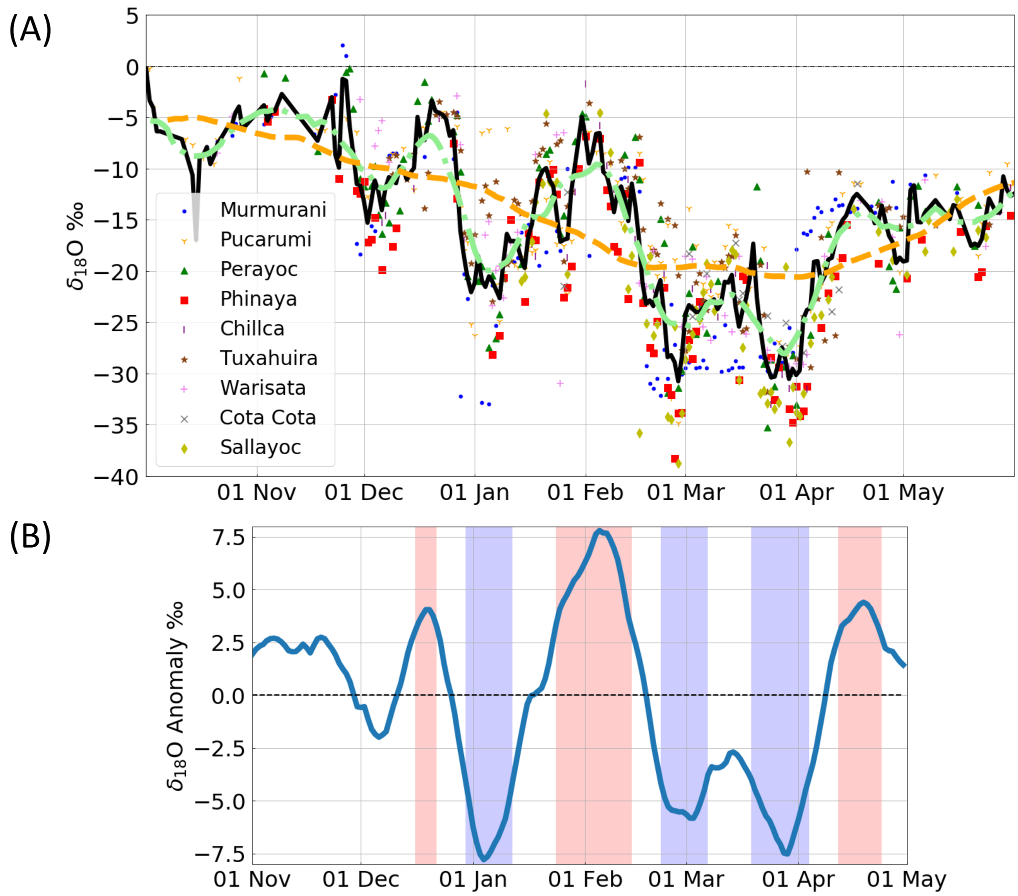

FIG. 5. A) δ^{18}O of all precipitation samples collected in 2017 (points, see legend inset), 3-day precipitation weighted mean of all samples (solid black line), 15-day moving average of the 30 day signal (dot-dash, green line, referred to as the subseasonal signal in this study) and the 90-day moving average of the 3-day signal (dashed, orange line, referred to as the seasonal cycle in this study). B) Subseasonal δ^{18}O anomalies during the 2017 wet season (subseasonal signal minus the seasonal cycle). Red shading highlights positive (+) anomalies where the δ^{18}O anomaly is above the 75th percentile for at least 5 days and blue shading highlights negative (-) anomalies where the δ^{18}O anomaly is below the 25th percentile for at least 5 days.

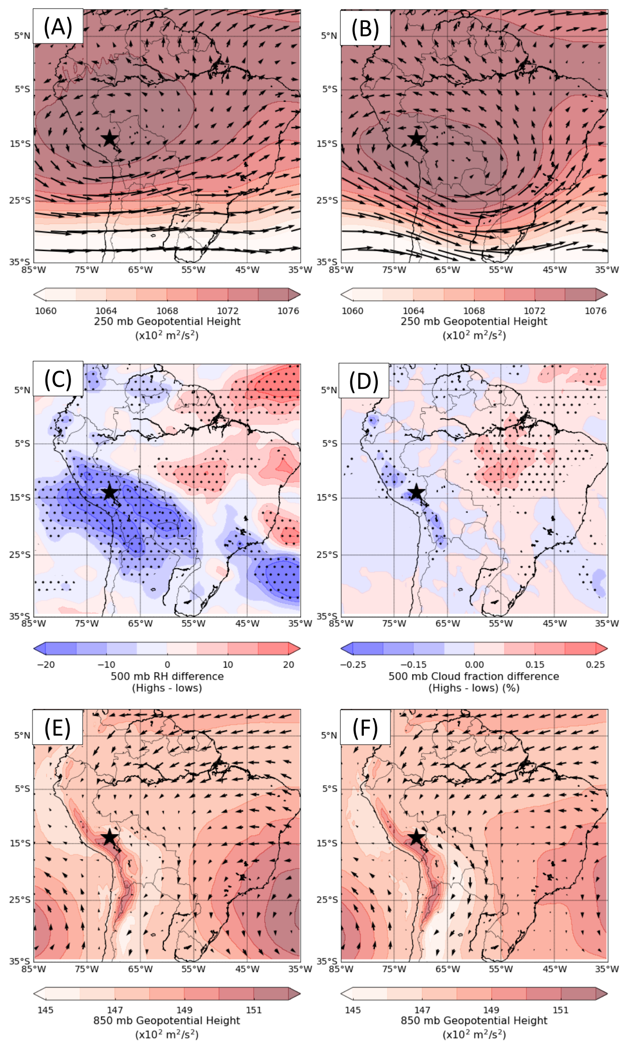

FIG. 6. Difference between positive and negative δ^{18}O anomalies in 2017. (A) and (B) show 250 hPa geopotential heights (contoured) and winds averaged over all of the positive anomalies and all of the negative anomalies respectively. (C) and (D) are difference plots, showing the average over all positive anomalies minus the average of all negative anomalies for 500 hPa relative humidity and 500 hPa cloud cover respectively. Black dots on the different plots show areas where the difference is significant at the 99% confidence interval. (E) and (F) show 850 hPa geopotential heights (contoured) and winds averaged over all of the positive anomalies and all of the negative anomalies respectively. The black star on each plot shows the location of Quelccaya in the Cordillera Vilcanota.

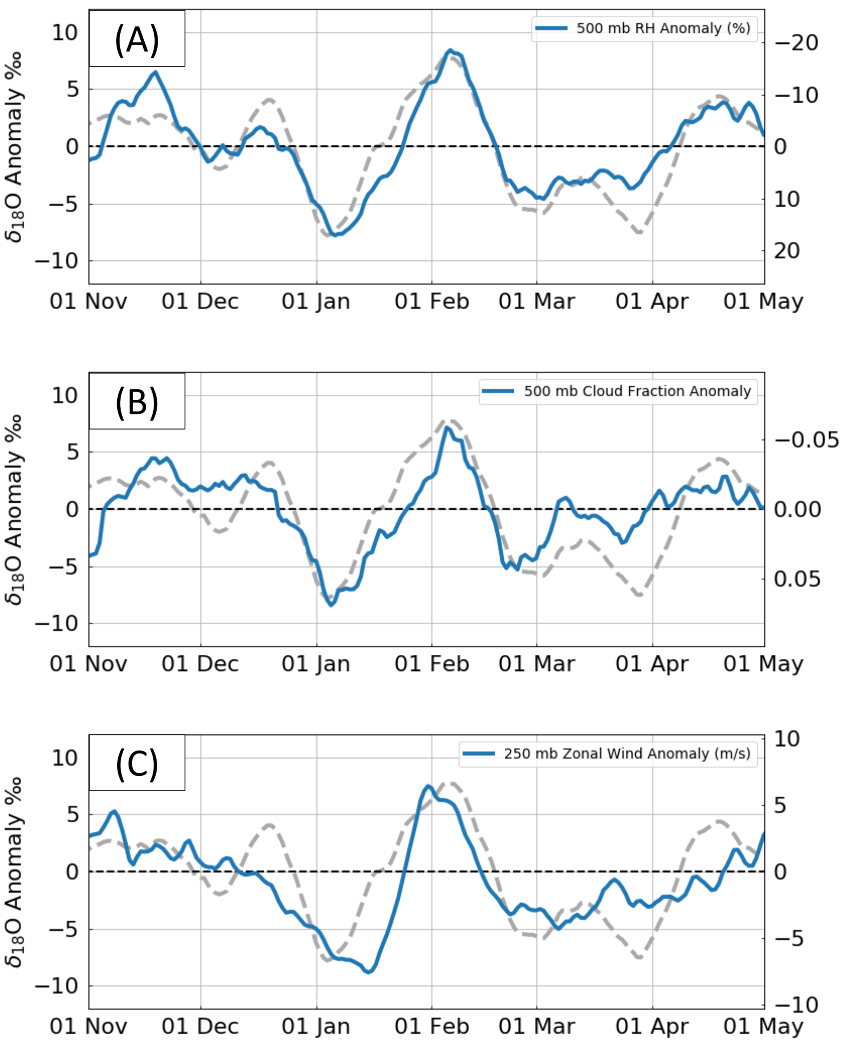

FIG. 7. 2017 time series of anomalies in (A) 500 hPa relative humidity, (B) 500 hPa cloud fraction and (C) 250 hPa zonal wind (solid blue line). Each anomaly series is calculated by subtracting the 90-day moving average (seasonal cycle) from the 15-day moving average of each field from ERA-Interim data averaged over the region 18.5° to 12° S and 74° to 65° W . The time series of δ^{18}O anomalies is overlaid on each plot for comparison (grey dashed line).

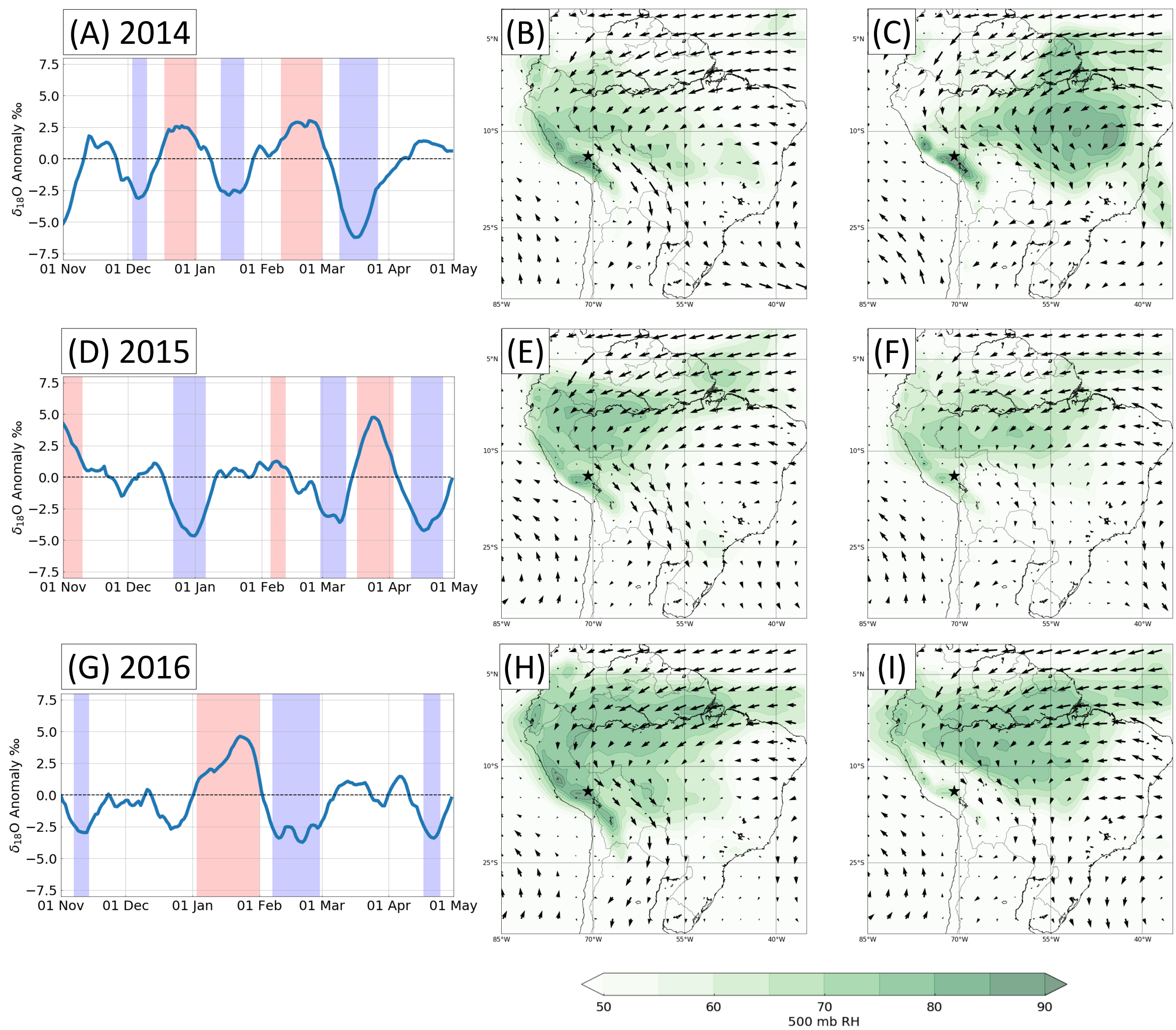

1120 FIG. 8. δ^{18}O anomaly plots for each wet season calculated in the same was as in Fig. 5b: (A) 2014, (D)
1121 2015, (G) 2016. Adjacent to each anomaly plot are spatial plots of 500 hPa relative humidity and 850 hPa winds
1122 averaged over each negative anomaly (B,E,H) and each positive anomaly (C,F,I) for each respective year. The
1123 black star on each spatial plot shows the location of Quelccaya

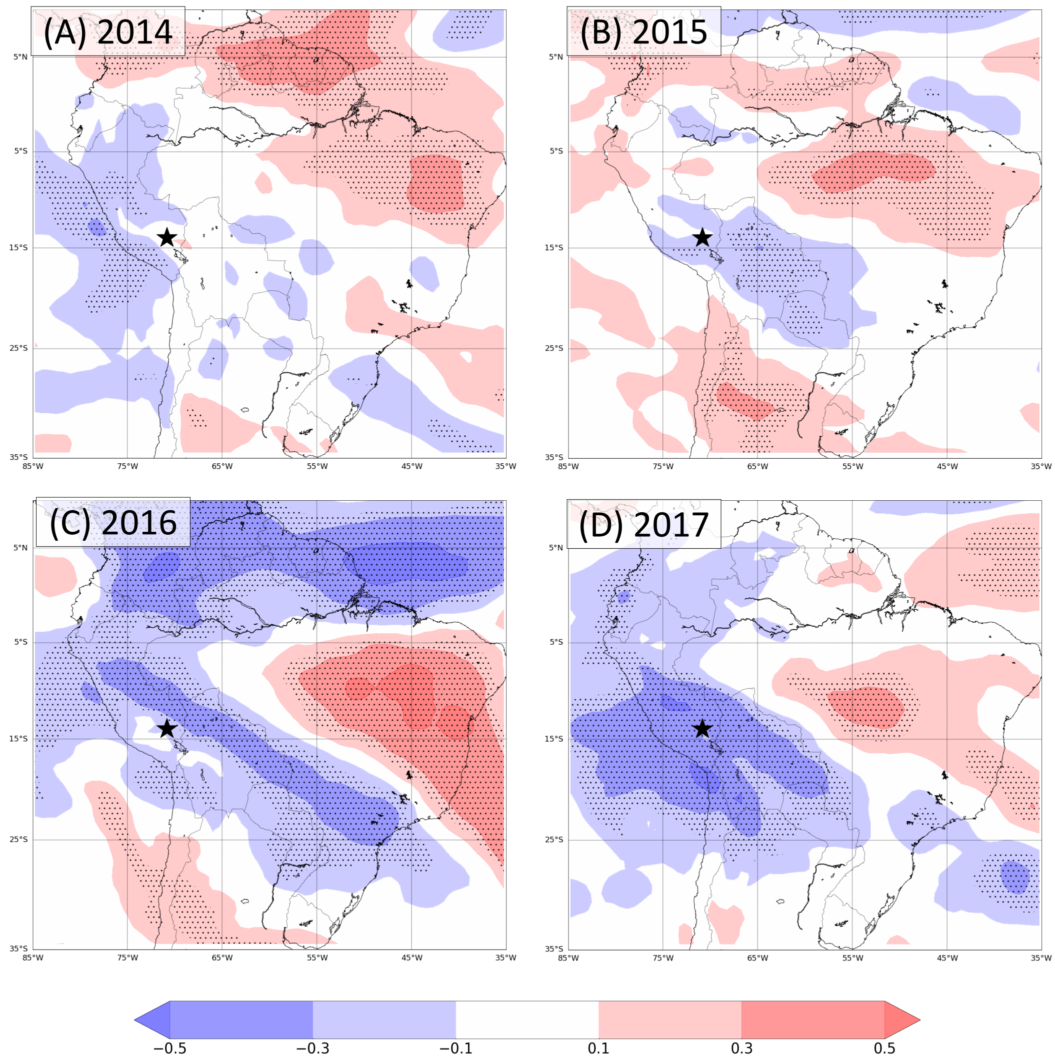

FIG. 9. Pearson's product-moment correlation coefficients between the time-series of δ^{18}O anomalies and time-series of 500 hPa relative humidity anomalies at every grid-point for each year. Black dots highlight areas where the correlation is significant at the 99% confidence level. On each plot the black star shows the location of Quelccaya.

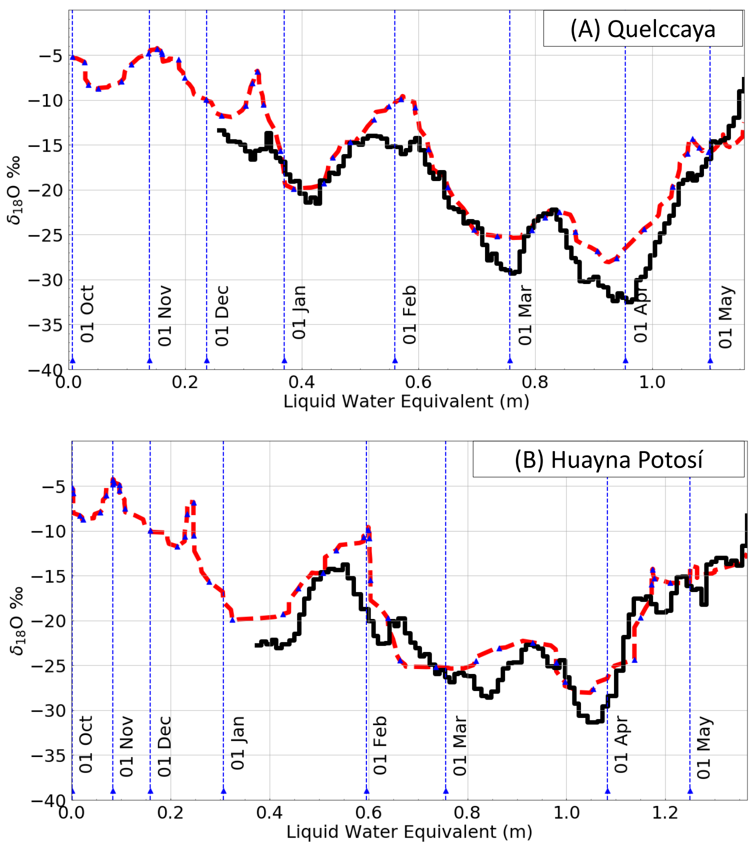

FIG. 10. δ^{18}O profiles of the annual layer snowpits on Quelccaya (A) and Huayna Potosí (B) sampled in July 2017. Overlain on each snowpit profile is the 15-day moving average δ^{18}O signal observed in region-wide precipitation, scaled to the liquid water equivalent depth in each snowpit from precipitation measurements from Quelccaya (A) and Chacaltaya (B), (red dashed line). Blue triangles are plotted every 5 days showing the snowpit age model. Vertical blue lines are plotted on the first day of each month.

Vita

Heather Guy was born in rural Lincolnshire in England where she attended Boston High School and achieved the highest grades in the school for A-levels in Maths, Physics, and Chemistry. On completion of her A-levels, she moved to Lancashire to study Natural Sciences at Lancaster University, specializing in Maths, Physics, and Environmental Science. In 2014, she had the opportunity to study abroad for a full year at the University of British Columbia in Vancouver, Canada, where she primarily took classes in the Department of Atmospheric Science and developed a passion for weather and climate. When she returned to England, she completed an internship at the U.K. Met Office where she developed a novel tool for assessing how well the Met Office high resolution forecast model simulated summertime convective precipitation. She finished her MSci degree back in Lancaster by completing a thesis investigating the potential to reduce the uncertainty in regional climate projections by incorporating stratosphere-troposphere coupling in global climate models.

On completion of her MSci, Heather spent a year travelling the globe volunteering on farms, completed two further internships related to weather forecasting and modelling, and spent some time working in a hotel in the Cumbrian Lake District. She moved to Boone, NC, in January 2017 to work as a graduate research assistant with Dr. Baker Perry at Appalachian State University to gain some experience doing research in the field. As part of this work, she has had the opportunity to go to Peru or Bolivia for fieldwork on four occasions, gaining experience in mountaineering and glacier travel, improving her Spanish, and participating in the exciting P2C2 research project, some of the results of which are communicated in this thesis.